מכון ויצמן למדע
WEIZMANN INSTITUTE OF SCIENCE

עבודת גמר (תזה) לתואר
דוקטור לפילוסופיה

מוגשת למועצה המדעית של
מכון ויצמן למדע
רחובות, ישראל

מאת
חגי אדרי

מדידות ספקטרוסקופיות של אינטראקציות בגזי בוז ופרמי מנוונים קוונטית

Thesis for the degree
Doctor of Philosophy

Submitted to the Scientific Council of the
Weizmann Institute of Science
Rehovot, Israel

By
Hagai Edri

Spectroscopic Measurements of Interactions in Quantum Degenerate Bose and Fermi Gasses

מנחים:
פרופ' ניר דודזון
פרופ' רועי עוזרי

Advisors:
Prof. Nir Davidson
Prof. Roee Ozeri

כסלו תש"פ

December 2019

Abstract

Mediated interactions are of broad interest in physics, ranging from high energy to condensed matter physics, and recently in systems of ultracold atoms [1–5]. All four fundamental interactions in the standard model have a bosonic mediators, which are elementary particles. In condensed matter and ultracold atoms, interactions are mediated by low energy excitations of the system which can be either of bosons or fermions and can change the ground state of the system and its phase.

In a metal, electrons can exchange phonons (excitations of vibration modes of the surrounding crystal) resulting in an attractive mediated interaction. At low temperatures this interaction leads to the formation of cooper pairs of electrons and BCS superconductivity. Electrons can also play the role of mediators, as two impurity ions in the crystal can exchange a fermion-hole excitation of the surrounding Fermi sea of electrons, leading to a long range Ruderman–Kittel–Kasuya–Yosida (RKKY) interaction [6–8]. Which was observed in solid state systems with spectroscopy measurements of the ion impurities [9]. RKKY interactions are of interest in other systems such as graphene, quantum dots and ultracold atoms. RKKY interaction can be intuitively understood - A boson immersed in a Fermi sea induces a perturbation to the fermion density that oscillates with a typical length inversely proportional to the Fermi wave-number k_f, known as Friedel oscillations [10]. When another boson interacts with the deformed Fermi sea, interaction is mediated between the bosons.

Ultracold atoms are a platform for measuring mediated interactions, the high degree of control in these systems allows for a direct measurement and control over the number of impurities, controlling the strength of interaction is possible with a Feshbach resonance. In a mean field approximation, the effect of mediated interaction is clear and can be measured with spectroscopy. There is an increasing interest in mediated interactions as a way of generating long range interaction between atoms, which can be used in different configurations to observe interesting phases and extending the Bose-Hubbard model [2].

We report on the first measurement of RKKY-like magnetic interaction between bosonic atoms in a Bose-Einstein Condensate which is mediated by virtual excitations of a quantum degenerate gas of fermionic atoms. Our observations were done using precision spectroscopy of the bosonic clock transition. We measured frequency shifts caused by interactions in our Bose-Fermi mixture and isolated the contribution of fermion mediated interaction. We measured an increase of spin-spin interaction between bosons by more than 40% in the presence of fermions. This result is in good agreement with theory and another recent mechanical measurement of a spinless analog of RKKY [4]. We also

measured an increase in the decoherence rate in the presence of fermions, another indication of mediated interaction.

Mediated interaction can lead to the future study of magnetic phase transitions and will allow for exploration of the physics of magnetic impurities in metals, such as the Kondo effect, using ultracold atomic gasses. Our method is general and can be used to measure other types of mediated interaction or close to a Feshbach resonance where the interaction diverges.

In the second part of this thesis, I describe a novel method for measuring interactions in a cold atomic cloud with unbalanced dynamic decoupling scheme. It is a general method that uses MW pulses to decouple the system from the environment and reduce noise while accumulating a phase due to inter species interactions between atoms. These interactions are of particular importance in polaron physics [11–14], where a minority of atoms in one state are strongly interacting with a majority of atoms in another state. Each minority atom is dressed by interacting with the other atoms, and it can be regarded as a quasi-particle with a finite lifetime known as polaron. Our method can also be used for spin squeezing, as it twists the Bloch sphere due to the interactions. We measure a scattering length difference between different states for three atomic transitions with high accuracy and high signal to noise ratio. Two of the transitions are magnetic sensitive, showing the strength of the method in overcoming strong magnetic noises.

Acknowledgments

The time I spent doing my PhD research was a very special period in my life. The cold bosons and fermions lab in room 183, in the complex system dept., in the physics faculty, in the Weizmann Institute of Science was the right place at the right time for me. I had many great people to work with and to learn from and it was a great experience. I came with a vague idea of what I wanted to do, but from the first few weeks here I knew I was with the right people around me and that it would be good idea spending time here. As time went by, and we had our fair share of difficulties along the way, I got more and more into it and when finally the research got going and we managed to achieve our humble goals, it was fun and exciting and it got more interesting.

My advisors Nir and Roee were incredible to work with, our discussions went on and on about everything that was happening in our lab in out of it. At first I thought we were being unproductive, discussing every small detail to great extent, and taking many detours to talk about other related issues as well, but I soon came to realize it was a lot more interesting and fun to do it this way and it gave us a much broader view on what were doing, and got us thinking about physics even when we were "in the trenches", as Roee likes to say. I've learned so much from both Nir and Roee and their broad scientific approach, they were so steady, positive and practical with their message and it helped us get going. They kept a good sense of humor about everything which eased the stress that usually comes with a PhD. They also gave me a lot of freedom in choosing what to do and how to do it, which is of special importance to me. Towards the end of my time here, it got more personal and I am grateful for spending a lot of time with two interesting, smart and curious individuals that helped me find my way.

Our experiment was always a group effort, making this complex machine work is a hard task that involves many people. It starts with the people that were with me in the lab, Asif Sinai, Noam Matzliah, Boaz Raz and Gavriel Fleurov who joined recently. Having a good lab partner is an important part of the work, as it is someone who really understands your ideas, your problems and your frustrations, and I have had great lab partners all along. I've learned a lot of things from their different approaches and while we didn't always agree on things (as it should be), there was always a good discussion, and i enjoyed working with them.

The group extends beyond the lab, to the other labs in the corridor, especially the cold bosons lab, the laser group of Nir and Asher, the Ions group of Roee and the Ofarim. It helped a lot to have that many people here that were struggling in a similar way and can provide and outsider look on

our research. It is not only that you can go into any room and ask any question you'd like, in most places you can just come and sit, and eventually someone will take his time to help you or just have a good conversation. I have to thank especially to Gadi Afek, Arnaud Corvoisier and Ravid Shaniv, with whom i had many fruitful discussions about research, life and everything in between.

The support team in complex systems dept. also has a part in the effort. The administrative staff in Weizmann always did their best to make things simple for us. The workshop and electronics guys, Guy, Gershon, Yuri, Rosty, Ezra and Meir were the best, we came to them with special requests, with short time restrictions, and they just delivered again and again. Only when I talked with people from other institutes and other departments I realized how many things they were doing for us and how good we have it here. Our lab would not function without their technical support and help.

Following my curiosity and pursuing a PhD research would not have been available to me without my family. My parents, Asher and Rosset Edri who always encouraged me to think and find what I like to do, and support me in every step I make no matter what it is. My bothers and sister, Eran, Yaron and Meital who were there to give advice and support as well.

A final word is to my wife and partner in life, Ilana, who has spent all this time with me, the good and bad times. Just her being there was a source of comfort and hope, knowing that I don't walk alone in this path. I couldn't do this without her endless support and love, and her way of knowing exactly what to say to get me out of my own head.

Contents

1 Introduction **7**

2 Experimental Setup **9**

2.1 A quantum degenerate Bose-Fermi mixture 10

2.2 Microwave and RF spectroscopy 12

2.2.1 Dynamic decoupling 16

3 Observation of Spin-Spin Fermion Mediated Interaction between Ultracold Bosons **18**

3.1 Theoretical Background 18

3.2 Experimental Results 24

4 Twisting the Bloch Sphere with Unbalanced Dynamic Decoupling **28**

4.1 Theoretical Background 28

4.2 Experimental Results 31

5 Summary and Outlook **37**

Chapter 1

Introduction

Experiments with ultracold atoms have become a fundamental tool in physics research. The first experimental realizations in 1995 of Bose-Einstein condensation (BEC) in dilute atomic gases [15, 16] marked the beginning of a very rapid development in this field. Ultracold dilute gas clouds provide a controlled and isolated environment to explore many-body physics phenomena, such as: bosonic and fermionic superfluids [17, 18], quantum phase transitions [19], supersolids [20–22], anti-ferromagnetism [23], many-body localization [24–26] and much more.

Experimentally these systems are attractive to work with, since atoms can be manipulated by lasers and magnetic fields with high precision. These tools are used to control the state of the system and reach interesting and non trivial quantum many-body states. A direct measurement of local properties that are not easily accessible in other many-body systems can be achieved by imaging the atoms momentum and position density. Tuning atomic interactions with Feshbach resonances [27, 28] is another powerful tool that allows experimentalists to challenge many-body theories and explore systems with long range correlations and strong interactions where theory is not available.

There is an ongoing effort in the cold atoms community to simulate condensed matter systems with ultracold fermions, some main examples are - artificial graphene with cold atoms [29], Haldane model [30], direct observation of anti-feromagnetic order on a microscopic level [23] and transport measurements of a bad metal [31]. Looking at these systems on the single atom level, using a quantum gas microscope [32–34], is another step in achieving a true quantum simulator, as proposed by Richard Feynman in the 1980s [35].

Interactions play a crucial role in these systems, as they change the physics from a single particle picture to a many-body problem. Ultracold atoms interact via Van der Waals potential, which is proportional to $\frac{1}{r^6}$ (where r is the distance between two atoms). In the ultracold regime, due to the low momenta and long wavelength of the atoms, only s-wave scattering is significant and the potential is well approximated by a contact potential ,$V_{VdW}(r) \underset{T\to 0}{\to} g\delta(r)$ where g is the interaction strength. When an atom scattered from many atoms around it, it gains a phase that is proportional to the density of atoms n, similar to light passing through a dielectric material. This phase is related to a mean field energy shift $\delta E_{mf} = gn$, it changes when atoms are in different internal states $|1\rangle$, $|2\rangle$

and causes density dependent frequency shifts for atomic transitions $\Delta f_{12} = \frac{1}{h}\left(\delta E^{(2)}_{mf} - \delta E^{(1)}_{mf}\right)$, here h is the Planck constant. While these shifts have an undesirable effect on atomic clocks that causes systematic errors in frequency [36–38], measuring them tells us about interactions in the system, and for strong interactions they can be used for spin squeezing [39].

My PhD work is centered around measuring these mean field frequency shifts in two different systems, a quantum degenerate mixture of bosons and fermions and a condensed Bose gas with imbalanced populations. In the first experiment (see chapter 3) we measured a mean field shift that stems form a spin-spin fermion mediated interaction between bosons, analogous to RKKY interaction in solids. Our experiment is similar to the first observations of such interaction in the 1950s and 1960s [9], where spectroscopic measurements of impurities in a crystal showed a dependence on the number of impurities. An observation that was later explained theoretically by Ruderman, Kittel, Kasuya and Yosida [6–8]. In our system we were able to change the number of bosons and measure frequency shifts with and without fermions, thus isolating the shift caused by mediated interaction. This interaction has a long range (decays as $\frac{1}{r^3}$) and it can be tuned using a Feshbach resonance, which can make it an exciting new tool in ultracold atoms experiments. Several theoretical proposals to observe interesting phases of matter using mediated interactions have been suggested [2, 3, 40].

In a second experiment we used a novel unbalanced dynamic decoupling scheme to measure a specific term in the frequency shift that is sensitive to population imbalance and inter-states interaction. Our method could be relevant for polaron physics as it allows to measure inter-states interactions with high precision and long coherence time. A polaron is a quasi-particle that emerges when a small number of atoms interacts strongly with a large reservoir of atoms, the minority atoms get dressed and form polarons. Originally suggested by Frohlich [41] for an electron moving in a solid state crystal, but recently observed in ultracold gasses in different settings [11–14] (Bose polaron, Fermi polaron etc.).

The sensitivity of the frequency shift to population imbalance generates an on axis twist in the Bloch sphere, which has been used for spin squeezing. While those measurements used strong interaction to get a spin squeezed state, we can use the long coherence time that is gained from dynamic decoupling to achieve that in the weak interaction regime.

In chapter 2 I describe our experimental setup, focusing on more recent improvements that allowed us to produce a quantum degenerate Bose-Fermi mixture, and explaining our spectroscopic techniques that were later used in the experiments. The main part of the thesis is a detailed description of our theoretical framework and experimental results for measuring fermion mediated interactions (chapter 3) and twisting the Bloch sphere with dynamic decoupling (chapter 4). I conclude in chapter 5 and propose some further research that can be done on these projects.

Chapter 2

Experimental Setup

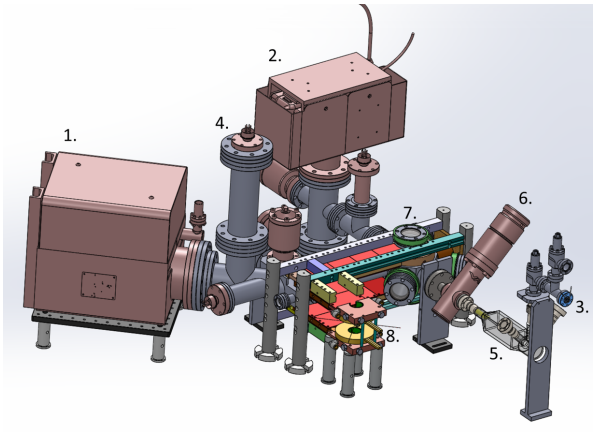

Figure 2.1: Schematic view of our experimental apparatus. Vacuum pumps (1-4) connected to three vacuum cells, - 2D MOT chamber (5), 3D MOT chamber (7) and science cell (8). The cells are connected with differential pumping tubes and a gate valve (6).

A detailed description of our experimental setup can be found in previous thesis in our group [42,43], I present here a short description and focus on the main advances in our setup over of the past two years, which allowed us to measure fermion mediated interaction in a Bose-Fermi mixture and perform dynamic decoupling using microwave (MW) pulses.

Our apparatus is built of three vacuum cells, a 2D-MOT (Magneto Optical Trap) cell connected to a 3D-MOT cell which is connected by an L shaped tube to a small glass cell (Science cell), the connections between the cells have a differential pumping section that allows for UHV in the 3D-MOT ($\sim 10^{-10}$ *torr*) and Science cell ($< 10^{-11}$ *torr*). A gate valve is placed between the 2D and 3D MOT cells which allows opening of the 2D MOT cell for changing dispensers.

The 2D-MOT cell is used to capture rubidium and potassium from vapor and cool it in two directions, and produces a beam of low velocity atoms moving towards the 3D MOT. Where we trap

and cool the atoms in all directions, we then compress the MOT and cool the atoms using Sisyphus cooling. After a short pulse of optical pumping to the stretched states of each atom, which are magnetically trappable, we turn on a quadrupole magnetic trap ($\sim 180\ G/cm$). Using 15 pairs of coils we move the magnetic potential electronically and transport the atoms adiabatically to the Science cell.

In the Science cell we trap the atoms in a strong quadrupole trap ($\sim 300\ G/cm$), which is then transformed into a quadrupole-Ioffe-configuration trap (QUIC) by turning on the current in another smaller coil. In this trap, which has a bias magnetic field of $\sim 4.6\ G$, we perform forced RF evaporation from a few hundred μK to $\sim 1\ \mu K$ in 38 Sec. The potassium atoms are not effected by the RF due to their lower Zeeman splitting by a factor of ~ 2.25, thus they are not removed by the evaporation and have to thermalize with the rubidium atoms to get colder (sympathetic cooling). At the end of this evaporation process the atoms are transferred to a crossed dipole trap, generated from a high power Nd:YAG laser (Mephisto 42W, at 1064 nm wavelength).

After a final stage of evaporation we have a Bose-Einstein condensate (BEC) of $\sim 5{\times}10^5\ ^{87}Rb$ atoms in at thermal contact with a degenerate Fermi gas (DFG) of $\sim 1.4 \times 10^5\ ^{40}K$ atoms in an harmonic trap of frequencies $\omega_{x,y,z} = 2\pi \times (\ 27, 39, 111)$ ($\omega_{x,y,z} = 2\pi \times (\ 29, 49, 182)$) for bosons (fermions) at a temperature of ~ 90 nK ($T/T_c \sim 0.55$ and $T/T_f \sim 0.35$, where T_c is the critical temperature of the BEC and T_F is the Fermi temperature of the DFG).

2.1 A quantum degenerate Bose-Fermi mixture

To get a quantum degenerate Bose-Fermi mixture we use forced evaporation a QUIC trap and a dipole trap. In the QUIC trap the evaporation is performed by an RF radiation that transfers the hottest rubidium atoms from a trapped state ($\mu > 0$) to an anti trapped state ($\mu < 0$) and thus removing them from the trap. After 2-3 collisions the atoms re-thermalize and get to a colder temperature. The potassium atoms are cooled by sympathetic cooling.

In the past our sympathetic cooling wasn't efficient enough and our potassium atoms would not cool down below $\sim 100\mu K$, due to a Ramsauer-Townsend minimum [44]) in the rubidium-potassium collision cross section and the short lifetime we had in the optically plugged magnetic trap due to magnetic noises in the 0-400 kHz range. Once we had a QUIC trap, our heating rate was lower and the lifetime was much longer which allowed a longer and more efficient evaporation. However, at some point we get similar number rubidium and potassium atoms and then sympathetic cooling is no longer efficient and we have to move the atoms adiabatically to a dipole trap where we evaporate by lowering the trapping potential depth for both species, thus potassium atoms are lost as well which allows us to continue cooling the mixture.

We get to quantum degeneracy after 38s evaporation in the QUIC trap and 5s evaporation in the dipole trap, which is probably a little longer than we could optimally but is more robust. We get a few 10^5rubidium and potassium atoms, with an almost pure BEC and $\frac{T}{T_F} \sim 0.25 - 0.35$. While the transition to a BEC is easily observed by looking at the momentum distribution of the rubidium

atoms as it changes from a Gaussian profile to an inverted parabola, the transition to a DFG is more subtle in a harmonic trap and effects mostly the edges of the momentum distribution. The momentum distribution for a thermal classical Boltzmann gas in a 3D harmonic trap is :

$$n\left(p\right)=\frac{N}{\left(2\pi mK_BT\right)^{3/2}}e^{-\frac{p^2}{2mK_BT}}$$

for a degenerate Fermi gas:

$$n\left(p\right)=-\frac{1}{\hbar^3\bar{\omega}^3}\left(\frac{K_BT}{2\pi m}\right)^{3/2}Li_{3/2}\left(-\mathfrak{Z}e^{-\frac{p^2}{2mK_BT}}\right)$$

After expanding for time t, and integrating in one dimension the optical density is:

$$OD\left(x,y\right)=\frac{\sigma_{cs}}{2\sqrt{\left(1+\omega_x^2t^2\right)\left(1+\omega_y^2t^2\right)}}\frac{m\left(K_BT\right)^2}{\pi\hbar^3\omega_z}Li_2\left(-\mathfrak{Z}e^{-\frac{x^2}{2\sigma_x^2}-\frac{y^2}{2\sigma_y^2}}\right)$$

where σ_{cs} is the absorption cross section, ω_i is the trapping frequency in axis i, $\bar{\omega}=\left(\omega_x\omega_y\omega_z\right)^{1/3}$, T is the temperature, m the atomic mass, N is the number of atoms, $\sigma_i=\frac{K_BT}{m\omega_i^2}\left(1+\omega_i^2t^2\right)$, and $\mathfrak{Z}$ is the fugacity. $Li_s(x)=\sum_{k=1}^{\infty}\frac{z^k}{k^s}$ is the Polylogarithm function. The differences between the distributions are small and are mostly seen around the tails of the distribution, we have to average azimuthaly over the image and fit to see a difference between the Gaussian and polylog profiles. We can also use the measured temperatures atom number and trap frequencies to estimate $\frac{T}{T_F}$ ($E_F=\hbar\bar{\omega}\left(6N\right)^{1/3}$). Our results show a clear indication of Fermi degeneracy in both methods, and their comparison is reasonable considering the accuracy of measuring number of atoms. We also measure the temperature of the bosons (the thermal part) and see that it is comparable to the temperature we get from the fermions.

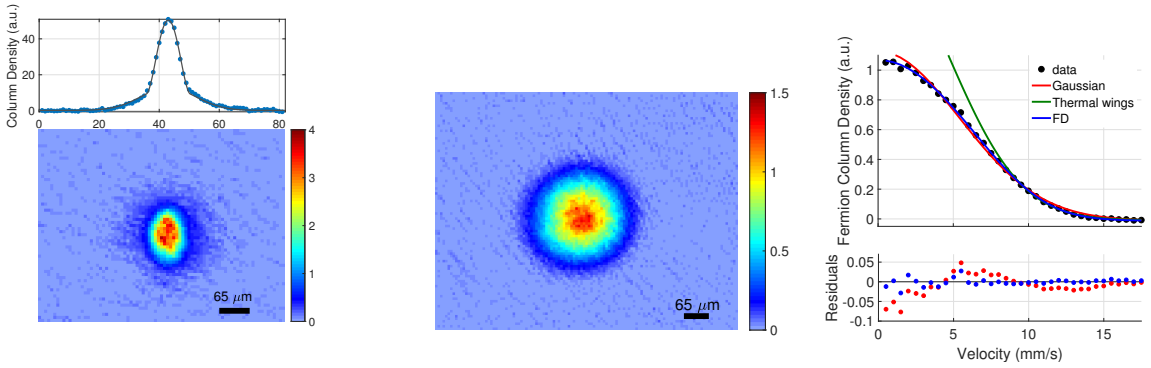

(a) (b)

Figure 2.2: Quantum Degenerate Bose-Fermi Mixture - (a) Image of a BEC after 20 ms time of flight, showing a high OD, anisotropic shape and bi-modal distribution in the column density (top panel). (b) Image of fermions after 12 ms time of flight (left panel) The fermions image shows a larger momentum distribution compared to the BEC and lower OD. After azimuthal averaging we can compare polylog fit to a Gaussian (right panel) and show it is indeed a degenerate Fermi gas. From the fit we get $\frac{T}{T_F}\Big|_{fit} = 0.29 \pm 0.01$ in good agreement with a calculation from number of atoms, trap frequencies, and temperature $\frac{T}{T_F}\Big|_{calc} = 0.3 \pm 0.05$.

2.2 Microwave and RF spectroscopy

To detect mean field frequency shift we use RF and microwave (MW) spectroscopy for potassium and rubidium respectively. We generate frequency from several homemade and commercially available frequency generators, all are locked to an atomic clock signal at 10 MHz to get long term stability. Our RF antenna is composed of two loops with a 5 cm diameter in Helmholtz configuration with ~ 5 cm distance from each side of the atoms. Our MW antenna is a horn antenna with a gain of $\sim 12dB$, both signals are amplified to ~ 10 $Watt$ before the antennas. We use frequency sweeps to get the atoms to the absolute ground state after loading them to the dipole trap from the magnetic trap, rubidium is in state$|F = 1, m_f = 1\rangle$ and potassium is in state $\left|F = \frac{9}{2}, m_f = -\frac{9}{2}\right\rangle$, where F is the total angular momentum and m_f is the spin projection on a quantization axis.

To detect population transfer in rubidium we use a normalized detection scheme , we take two consecutive images with a short repump pulse between them to get all atoms to $F = 2$ manifold. In the first image only atoms in $F = 2$ are imaged, and in the second image we image all of atoms, from the 2 images we get $P = \frac{N_2}{N_1+N_2}$ (where $N_{1,2}$ is the number of atoms in $F = 1, 2$ manifolds). To detect populations in different spin states we use a Stern Gerlach (SG) measurement where we release the atoms from the trap and let them expand with a magnetic field gradient so each states appears in a different position in the image.

Our MW spectroscopy is done on the hyperfine levels of rubidium at 6.834 GHz, we use magnetic sensitive ($|1, 1\rangle \rightarrow |2, 2\rangle$,and $|1, 1\rangle \rightarrow |2, 0\rangle$) and magnetic insensitive transitions ($|1, 0\rangle \rightarrow |2, 0\rangle$, clock transition). With one MW pulse we perform Rabi pulse length scan and frequency scans (Figure 2.3)

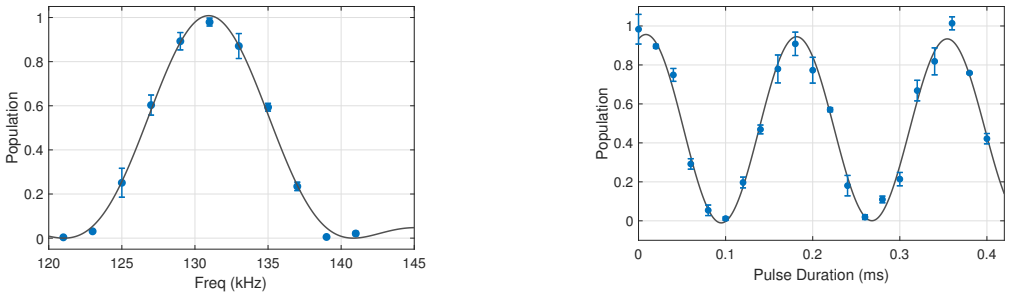

(a) (b)

Figure 2.3: Rabi Spectroscopy - (a) Rabi Spectrum for $|1,1\rangle \rightarrow |2,0\rangle$ transition with a pulse length of 98 μS . The spectrum is power broadened and has a the shape of $sinc^2(x)$ function with a width of $\sim 5\ kHz$, the pulse is a squared pulse. The displayed frequency is the detuning from the $|1,0\rangle \rightarrow |2,0\rangle$ transition at 6.834682 GHz. (b) Rabi oscillations on the clock transition $|1,0\rangle \leftrightarrow |2,0\rangle$, the atoms start at $|2,0\rangle$ and oscillate between the 2 states with a Rabi frequency of $\sim 5\ kHz$, an almost full contrast shows we have all the atoms in a single spin state.

to calibrate our pulse length and frequency and detect magnetic field fluctuations over time. With two pulses separated by a Ramsey time t_R we perform Ramsey time scans to detect frequency shifts (Figure 2.4) on the clock transition. In a Ramsey time scan we usually use a detuning of 150 Hz compared to the transition frequency at zero magnetic field.

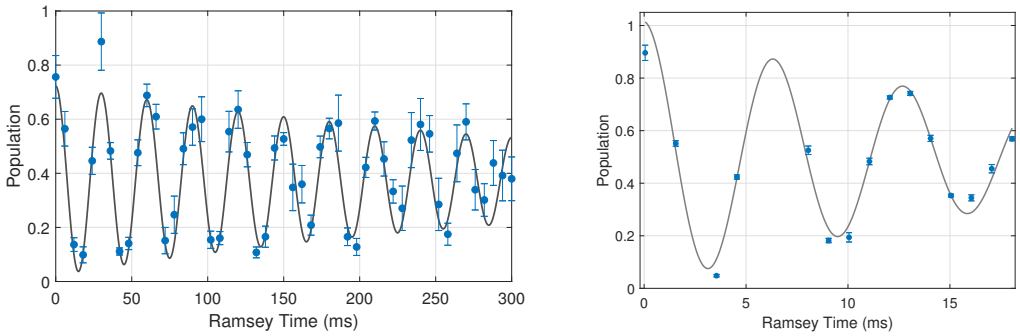

(a) (b)

Figure 2.4: Ramsey Spectroscopy - Evolution of the population in the $|2,0\rangle$ while scanning the Ramsey time between 2 pulses on the clock transition with a constant detuning. (a) For a thermal cloud at a temperature of $\sim 0.6\ \mu K$, decay time is ~ 0.5 sec. (b) For a pure BEC, decay time is ~ 20 ms. Decay of the signal a BEC is much faster, indicating the main source of decoherence is inhomogeneous density frequency shifts in a BEC. We use this type of measurement with/without fermions and for different boson densities to measure boson-fermion frequency shifts and mediated interactions.

We use Ramsey spectroscopy on magnetic sensitive transitions to detect 50 Hz noise in our lab. For this measurement we synchronize our pulses to the 50 Hz signal from the power grid in our lab.

We then perform a Ramsey sequence with constant Ramsey time and scan the phase of the second pulse. We change the time delay between the 50 Hz signal and the MW pulses (figure 2.5)and get a phase shift that is related to the amplitude of the 50 Hz signal $\delta\phi = (\mu_2 - \mu_1) B_{50}$, here $\delta\phi$ is the peak to peak phase shift over our time delay scan, $\mu_{1,2}$ are the magnetic moments of the atomic states and B_{50} is the peal to peak magnetic noise at 50 Hz. We get 0.89 mG peak to peak amplitude of the magnetic field at 50 Hz, we do not detect any other significant noise frequencies in our measurements.

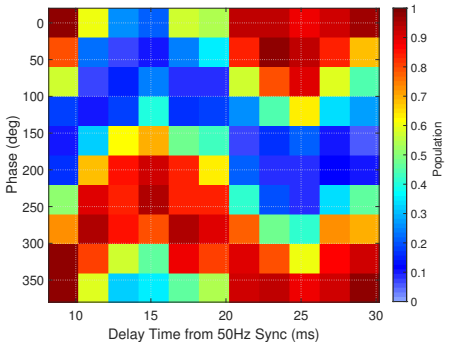

Figure 2.5: 50 Hz Noise - Ramsey phase scan with Ramsey time of $0.8ms$, magnetic sensitive transition $|1,1\rangle \rightarrow |2,0\rangle$. Changing the delay time between our |Ramsey pulses and 50 Hz square pulse we get from the electricity network in our lab. We measure a phase shift that is proportional to the magnetic field noise at 50 Hz as seen by the atoms. We get 0.89 mG peak to peak amplitude of the magnetic field at 50 Hz, with no major components at multiples of 50 Hz.

We use RF spectroscopy to transfer potassium to its ground state. To measure spin states of potassium we release the atoms from the trap and apply a strong magnetic field gradient to separate the states during time of flight (a Stern Gerlach measurement), using RF field we can drive transitions from $\left|\frac{9}{2}, -\frac{9}{2}\right\rangle \leftrightarrow \left|\frac{9}{2}, +\frac{9}{2}\right\rangle$ and follow the clouds position in the image (Figure 2.6). Rf pulses are part of our future plan to use a scheme interleaved dynamic decoupling on rubidium and potassium together to measure mediated interaction (see more detail in summary and outlook).

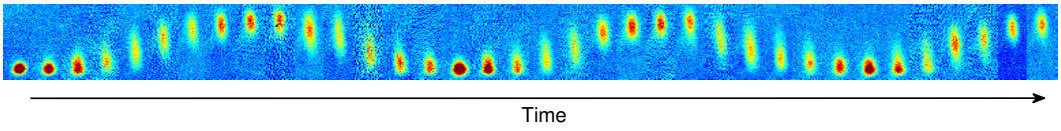

Figure 2.6: RF Rabi Oscillation - Fermions images after time of flight in a constant magnetic gradient (Stern Gerlach) for different RF pulse lengths. The atoms start at the bottom of the image (state $\left|\frac{9}{2}, -\frac{9}{2}\right\rangle$) and gradually move to the top of the image (state$\left|\frac{9}{2}, \frac{9}{2}\right\rangle$) through different superposition of spin states. Time difference between 2 consecutive images is 10 μS. The cloud size and position are used to identify pure spin states.

For a long time we have suspected we have RF noise in our lab in the range of $10 - 1000\ kHz$. To measure it we start our rubidium atoms in state$|1,1\rangle$ in the dipole trap and wait in a constant magnetic field B for time $t_{hold} \sim 2s$ and perform a Stern Gerlach measurement to see if some of the atoms transferred to a different spin state due to RF noise in our lab. By scanning the magnetic field and hold times we could measure the spectrum and strength of our RF noise (Figure 2.7). To find the source of the noise we tried measuring it with a magnetic coils in different places in the lab, we found that the noise is caused mostly by switching power supplys that create noise to the electrical ground in our lab. This noise is radiated on the atoms by the trap coils, to avoid it we had to physically disconnect the coils from the ground by relays, as IGBTs and MOSfets can let noise at RF frequencies pass. Our future plan is to change all the power supplies to linear ones that have much less ground noise.

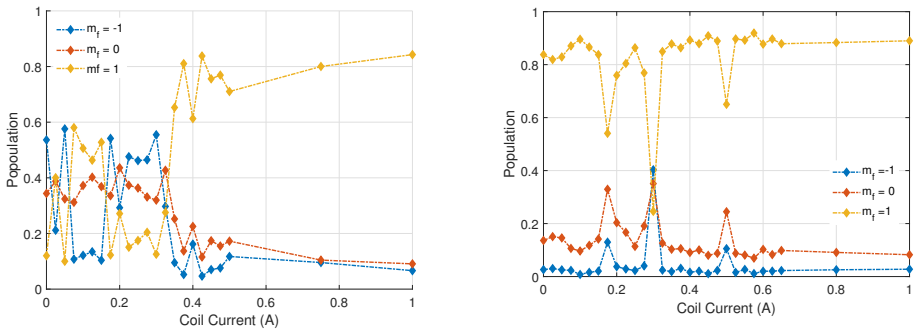

(a) (b)

Figure 2.7: RF Noise Spectrum - Population of rubidium atoms after 2s holding time in different magnetic fields, controlled by the current in pair of Helmholtz coils. Atoms start at a state $m_f = 1$, RF noise transfers them to other states. (a) In our first measurement the noise was very wideband, and we get a mixed states in currents up to 0.45 A ($\sim 500\ kHz$). (b) After disconnecting the trap coils from the ground with relays, and changing some power supplies in the lab, we reduce the noise in most frequencies and only several peaks of noise at specific frequencies remained. We could not find a specific source for those frequencies.

2.2.1 Dynamic decoupling

Dynamic decoupling is a well known method for decoupling a system from its environment and conserving its state for long times. It applies to classical and quantum systems, and has been demonstrated in NMR [45–47], spins in solids [48, 49], trapped ions [50–54] and ultracold atoms [55, 56] (and can also be done with a simple hourglass!). In a quantum 2-level system, the simplest form of dynamic decoupling is adding a π pulse in the middle of the Ramsey sequence - Han echo [57]. The sequence is a $\pi/2$ pulse - wait time T_{arm}- π pulse - wait time T_{arm} - $\pi/2$ pulse. Each state gets a phase according to its energy $E_{1,2}$, and because of flipping the states with a π pulse, both states get the same phase (global phase) and coherence is conserved. This holds true as long the phase gained on both arms of the echo is equal, it can be different if the environment or system changes during the sequence.

The evolution of the state between the $\pi/2$ pulses is :

$$\frac{1}{\sqrt{2}}\left(|1\rangle+|2\rangle\right)\xrightarrow{T_{arm}}\frac{1}{\sqrt{2}}\left(e^{-i\frac{E_1}{\hbar}T_{arm}}|1\rangle+e^{-i\frac{E_2}{\hbar}T_{arm}}|2\rangle\right)\xrightarrow{\pi\text{ pulse}}\frac{1}{\sqrt{2}}\left(e^{-i\frac{E_1}{\hbar}T_{arm}}|2\rangle+e^{-i\frac{E_2}{\hbar}T_{arm}}|1\rangle\right)$$
$$\xrightarrow{T_{arm}}\frac{1}{\sqrt{2}}e^{-i\left(\frac{E_1}{\hbar}+\frac{E_2}{\hbar}\right)T_{arm}}\left(|1\rangle+|2\rangle\right)$$

it is clear that the state only gets a global phase as long as $E_{1,2}$ are constant during the sequence. This sequence cancels Zeeman energy shifts (due to magnetic field) or light shifts if they are the same in both arms of the echo, but it also cancels any density shift that is the same in both arms. We perform an unbalanced dynamic decoupling scheme (see section 4.1) to cancel all quasi-static noises and accumulate a phase due to frequency shifts that depend on density difference between the states.

To perform dynamic decoupling we use a home built MW frequency source that generates a signal in the range 6.8-7.2 GHz, it is locked to a 10 MHz rubidium clock frequency standard (SRS FS725). Our source has digital control over its phase, which allows for an accurate scan of the phase of the last pulse in the sequence and changing the phase of the π pulses to avoid control errors.

With dynamic decoupling we are able to increase our coherence time for the clock transition from $\sim$ 15 ms to $\sim$ 100 ms (figure 2.8) . We have successfully used up to 72 echo pulses on magnetic sensitive hyperfine transitions to achieve a long coherence time of $\sim$ 100 ms in the presence of strong 50 Hz noise (peak to peak $\sim$ 1 mG), where a Ramsey measurement loses coherence after a short time ($<$ 1ms).

When using many echo pulses, it is important to avoid errors in the pulses itself as they will accumulate over time and lead to decoherence. There are many schemes to optimize coherence time and avoid errors [58, 59], in our measurements (chapter 4)we use an XY8 sequence, each block has 8 pulse, ordered as: $X\ Y\ X\ Y\ Y\ X\ Y\ X$, here $X(Y)$ means a π pulse around the X (Y) axis in the Bloch sphere, there is a phase shift of 90° between the two.

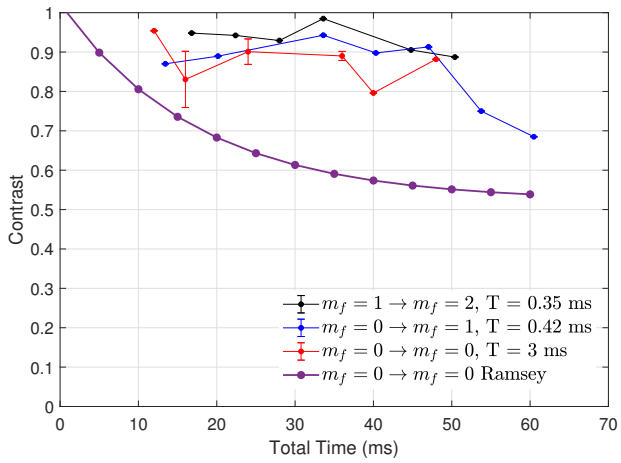

Figure 2.8: Coherence in Dynamic Decoupling - Fringe contrast after dynamic decoupling sequence for three transitions with a constant arm time and increasing number of pulses.$|1,0\rangle \rightarrow |2,0\rangle$ tranisition with arm time $T = 3$ ms (red) $|1,1\rangle \rightarrow |2,0\rangle$tranisition with arm time $T = 0.42$ ms (blue), and$|1,1\rangle \rightarrow |2,2\rangle$ tranisition with arm time $T = 0.35$ ms (black). Contrast from fit to Ramsey measurement of $|1,0\rangle \rightarrow |2,0\rangle$ transition is plotted for comparison (purple). The coherence is kept high for long times for all transition, it is perserved even in the presence of strong 50 Hz magnetic noise for the magnetic sensitive transitions (blue, black).

Chapter 3

Observation of Spin-Spin Fermion Mediated Interaction between Ultracold Bosons

This chapter details the main experimental result of this work [5]. We used MW Ramsey spectroscopy to detect frequency shifts related to mean field interactions in a quantum degenerate Bose-Fermi mixture. We measured these shifts as a function of boson density, with and without fermions, and distinguished three main contributions - boson-boson interactions, boson-fermion interaction and fermion-mediated interaction. Our results show a clear sign of spin-spin fermion mediated interaction between the bosons, in the frequency shift and decoherence rate of the Ramsey signal. We also measured the boson-fermion frequency shift for the first time, which can be used to calibrate inter-atomic potentials.

3.1 Theoretical Background

The effect of mediated interactions in cold atoms can be calculated in several ways - linear response theory, 2nd order perturbation [1,2] and path integrals [60]. It was proposed as a new approach to create long range interactions similar to systems of polar molecules or highly magnetic atoms. Following [2], a 2nd order perturbation theory for RKKY interaction in an ultracold Bose-Fermi mixture of atoms is presented, along with mean field frequency shifts due to mediated interaction in this mixture in a 3D harmonic trap.

Interactions in an ultracold boson-fermion mixture are manifested by elastic collisions. In a system of a condensed Bose gas (^{87}Rb) and spin polarized degenerate Fermi gas (^{40}K), the collisions between the bosons and fermions lead to an effective long-range interaction between the bosons, analogous to Ruderman–Kittel–Kasuya–Yosida (RKKY) interaction in solids [6–8].

Consider a system of two bosonic ^{87}Rb atoms immersed in a polarized degenerate Fermi gas of ^{40}K at $T = 0$, the non-interacting state of the system is $|g\rangle = |\Psi_B(k_1, k_2)\rangle \bigotimes |\Psi_{DFG}\rangle$ with energy

$E_g = \frac{\hbar^2(k_1^2+k_2^2)}{2m_B} + \frac{3}{5}N_F\varepsilon_F$, $k_{1,2}$ are the bosons momenta ,m_b - boson mass , N_F, ε_F are the fermion number and Fermi energy. The spin polarized fermions do not interact between themselves at low temperature due to Pauli exclusion principle, however, they can collide with one of the bosons, creating a particle-hole excitation of the Fermi gas which can propagate and interact with the second boson. This process gives rise to an effective potential between the bosons.

The boson-fermion (rubidium-potassium) and boson-boson (rubidium-rubidium) collisions are described by a contact interaction Hamiltonians:

$$\hat{H}_{BF} = g_{bf}\int d^3r\psi_b^\dagger(r)\psi_f^\dagger(r)\psi_b(r)\psi_f(r)$$

$$\hat{H}_{BB} = \frac{g_{bb}}{2}\int d^3r\psi_b^\dagger(r)\psi_b^\dagger(r)\psi_b(r)\psi_b(r)$$

where $g_{bf} = 2\pi\hbar^2 a_{bf}\left(\frac{1}{m_{Rb}}+\frac{1}{m_K}\right)$, $g_{bb} = \frac{4\pi\hbar^2}{m_{Rb}}a_{bb}$, a_{bf} (a_{bb}) is the boson-fermion (boson-boson) s-wave scattering length and $\psi_b^\dagger\left(\psi_f^\dagger\right)$ are the boson (fermion) creation operators. The effective Hamiltonian describing the mediated interaction is:

$$H' = \sum_{\{k_1,k_2,k_1',k_2'\}} |g(k_1,k_2)\rangle \left[\sum_{|e\rangle}\frac{\langle g|\hat{H}_{BF}|e\rangle\langle e|\hat{H}_{BF}|g\rangle}{(E_e-E_g)}\right]\langle g(k_1',k_2')|$$

The sum over $\{k_1,k_2,k_1',k_2'\}$ is when the fermions are in their ground state $|\Psi_{DFG}\rangle$, and the sum over states $|e\rangle$ is when the fermions are in an excited state. In the case of light fermions - $m_f \ll m_b$, here m_f $(m_b)$is the fermion (boson) mass, one can integrate out the fermionic degrees of freedom and get a boson-boson potential. After calculating the sums (for details see [2]) the effective interaction and potential are:

$$H' = \frac{1}{2}\int d^3\{r_1,r_2\}\psi_b^\dagger(r_1)\psi_b^\dagger(r_2)V(r_1-r_2)\psi_b(r_2)\psi_b(r_1)$$

$$V(R) = -\xi\frac{2m_f g_{bf}^2 k_F^4}{\pi^3\hbar^2}\frac{\sin(2k_FR)-2k_FR\cdot\cos(2k_FR)}{(2k_FR)^4}$$

$k_F = \frac{\sqrt{2m_F\varepsilon_F}}{\hbar}$ is the Fermi momentum and ξ is a dimensionless factor that was calculated to be 1 [1]or π^3 [2]. This potential is shown in figure 3.1 and is identical to the RKKY interaction in solids. It is a long range potential $\propto R^{-3}$ for $R \gg k_F^{-1}$, and oscillates at $2k_F$. This oscillation results from an oscillation in the fermion density caused by the presence of the boson, known as Friedel oscillations [10].

In our experiment the mixture is held in a 3D harmonic trap at sub-micro Kelvin temperature. We use a mean field approximation to calculate the energy shift caused by the mediated interaction. The mediated interaction is characterized by an effective mediated boson-boson coupling $g_{med} =$

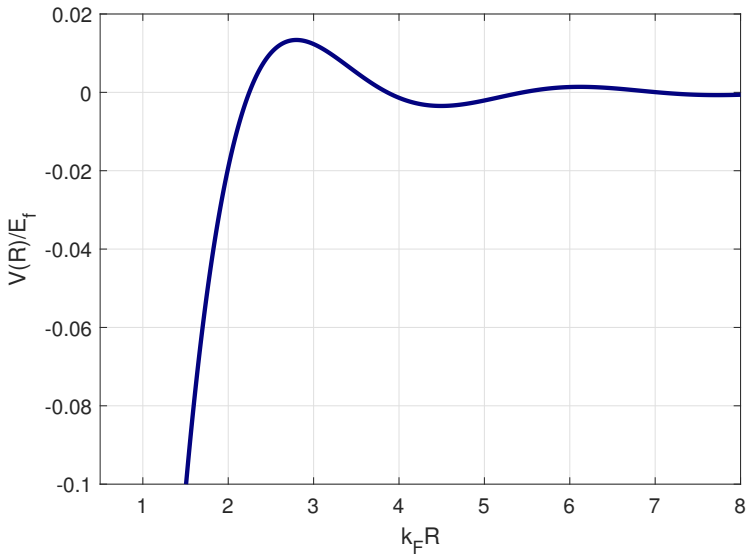

Figure 3.1: Fermion Mediated Boson-Boson Interaction - Mediated interaction potential in units of Fermi energy, R is the distance between bosons.

$\int d^3RV(R)$, and an effective scattering length a_{med} :

$$g_{med} = \frac{4\pi\hbar^2}{m_B} a_{med}, \quad a_{med} = -\frac{\xi}{2\pi} \frac{(m_b + m_f)^2}{m_b m_f} \left(6\pi^2 n_f\right)^{1/3} a_{bf}^2$$

The scattering length is proportional to $n_f^{\frac{1}{3}}$ and to $-a_{bf}^2$, thus it is always attractive. For two bosons in different spin states ($e.g.$ $\uparrow,\downarrow$) the interaction will be $g'_{\downarrow\uparrow} \propto g_{\downarrow f} \cdot g_{\uparrow f}$ which can be repulsive or attractive, depending on the signs of the boson-fermion interaction $g_{\downarrow f}$, $g_{\uparrow f}$. In the mean field approximation, the energy shift due to interactions will be $E_{bb} = \frac{4\pi\hbar^2}{m_b} n_b a_{bb}$ - boson-boson interaction , $E_{bf} = 2\pi\hbar^2 \left(\frac{1}{m_b} + \frac{1}{m_f}\right) n_b a_{bf}$- boson-fermion interaction, and $E_{bb} = \frac{4\pi\hbar^2}{m_b} n_b a_{med}$ - fermion-mediated interaction.

There are three main issues concerning this interaction in our system :

1. The mass ratio is not large - in our setup we only have $\frac{m_b}{m_f} \sim 2$, but because our bosons are in a BEC with a chemical potential of $\sim 65\ nK$ and the relevant fermions for this interaction have energy close to the Fermi energy $\sim 260nK$, the change in fermion energy $\Delta\epsilon_f$ is larger than the change in boson energy $\Delta\epsilon_b$. For a momentum change q , smaller than the Fermi momentum k_f ,the energy change ratio is $\Delta\epsilon_f/\Delta\epsilon_b \sim \frac{m_b}{m_f}\frac{k_f}{q} \gg 1$.

2. The long range nature of the potential means that all partial waves should be taken into account in the scattering process. Due to the low energy of the condensate we assume that the main contribution will be from the s-wave collisions, since the de-Broglie wavelength λ_{dB} of the bosons is much longer than the potential range $\sim (2k_F)^{-1}$, with our parameters $2k_F\lambda_{dB} \sim 15$.

More generally, any change in the frequency shift that is not linear can also be detected in our measurement.

3. Our Fermi gas is not at zero temperature. This means that the Friedel oscillations should be averaged out to some extent. However, since we are looking at the average mean field effect of RKKY interaction we are insensitive to that.

Direct mean field calculation of mediated interaction

I present here another way to calculate this interaction in the mean field approximation, which is a more simple perturbative approach that gives the same result.

The chemical potential of a BEC and a DFG in a mixture at zero temperature is:

$$\mu_b = g_{bb}n_b + g_{bf}n_f,\ \mu_f = \frac{\hbar^2 k_f^2}{2m_f} + g_{bf}n_b$$

using $k_f = \left(6\pi^2 n_f\right)^{1/3}$we can turn the second equation to get $n_f = \frac{1}{6\pi^2}\left(\frac{2m_f}{\hbar^2}\left(\mu_f - g_{bf}n_b\right)\right)^{3/2}$, plugging it into the above equation we get:

$$\mu_b = g_{bb}n_b + g_{bf}\frac{1}{6\pi^2}\left(\frac{2m_f}{\hbar^2}\left(\mu_f - g_{bf}n_b\right)\right)^{3/2}$$

assuming the boson fermion interaction is a small perturbation to the Fermi gas chemical potential $\left(\frac{g_{bf}n_b}{\mu_f} \ll 1\right)$ we can use Taylor expansion to get $\mu_b \approx g_{bb}n_b + g_{bf}\frac{1}{6\pi^2}\frac{2^{3/2}m_f^{3/2}}{\hbar^3}\mu_f^{3/2}\left(1 - \frac{3}{2}\frac{g_{bf}n_b}{\mu_f}\right)$.

At the lowest order approximation we can use the unperturbed fermion chemical potential which is just the Fermi energy $\mu_f^0 = E_F = \frac{\hbar^2 k_f^2}{2m_f} = \frac{\hbar^2\left(6\pi^2 n_f^0\right)^{2/3}}{2m_f}$to get :

$$\mu_b = g_{bb}n_b + g_{bf}n_f^0 - \frac{1}{2\pi^2}\frac{m_f}{\hbar^2}\left(6\pi^2 n_f^0\right)^{1/3} g_{bf}^2 n_b$$

From this result we can understand the effect of fermions on the BEC, the first term is the boson-boson interaction, the second term is the direct boson-fermion interaction and the third term is the fermion-mediated interaction. It is proportional to g_{bf}^2, $n_f^{1/3}$ and n_b just like we got in the more elaborate calculation. We can now recognize that:

$$g_{med} = -\frac{1}{2\pi^2}\frac{m_f}{\hbar^2}\left(6\pi^2 n_f\right)^{1/3} g_{bf}^2$$

which exactly what we got before for $\xi = 1$.

Mean field frequency shift

To measure the effect of mediated interaction we look at the frequency shift of the ^{87}Rb hyperfine transition. These energy levels are shifted due to interactions, the effect of the mediated interaction between the bosons should cause an additional shift on-top of the boson-boson and boson-fermion frequency shifts. There are three main parameters that change these effects: fermion density, boson density and the bare boson-fermion scattering length a_{bf} (can be tuned using a Feshbach resonance [61]). In the following I estimate the frequency shift for different boson densities at zero magnetic field for the transition $|F=1,m_f=0\rangle \rightarrow |F=2,m_f=0\rangle$ (clock transition). This transition has no first-order Zeeman shift at low magnetic fields and therefore is insensitive to magnetic noises. The mean-field shift of the transition frequency between two hyper-fine states of the bosons in a BEC :

$$\Delta f = \underbrace{2\frac{\hbar}{m_b}\left(a_{bb_2}-a_{bb_1}\right)n_b}_{\Delta f_{bb}} + \underbrace{\hbar\left(\frac{1}{m_f}+\frac{1}{m_b}\right)\left(a_{bf_2}-a_{bf_1}\right)n_f}_{\Delta f_{bf}} + \underbrace{2\frac{\hbar}{m_b}\left(a_{med_2}-a_{med_1}\right)n_b}_{\Delta f_{med}} \tag{3.1}$$

a_{bb_i}, a_{bf_i}, a_{med_i} are the boson-boson, boson-fermion and mediated interaction scattering length of the two hyper-fine states respectively.

The frequency shift between two hyper-fine levels includes three contributions - boson-boson interaction Δf_{bb}, boson-fermion interaction Δf_{bf} and mediated interaction Δf_{med}. Δf_{bb} and Δf_{med} are proportional to boson density, while Δf_{bf} is independent of it. Δf_{med} can be controlled by changing the boson density or the boson-fermion scattering length using a Feshbach resonance (changing the fermion density is less favorable as Δf_{med} is only proportional to $n_f^{1/3}$). To distinguish between the three contributions, we measure frequency shift for different boson densities, with and without fermions. With only bosons present, we measure Δf_{bb}, the change in frequency per boson density $\left(\frac{\mathrm{d}\Delta f}{\mathrm{d}n_b}\right)_b$ is a measure of boson-boson interaction. When we add fermions, we get a constant term Δf_{bf} that does not depend on boson density and Δf_{med}, which causes change in frequency that is proportional to boson density. A change in the slope $\left(\frac{\mathrm{d}\Delta f}{\mathrm{d}n_b}\right)_{b+f}$ (measurement with bosons and fermions) compared to $\left(\frac{\mathrm{d}\Delta f}{\mathrm{d}n_b}\right)_b$ (measurement with bosons only) is a clear indication of fermion mediated interactions between bosons in our mixture.

To estimate the frequency shift one must know the scattering lengths a_{bf_2}, a_{bf_1} and $a_{bb_2}-a_{bb_1}$, we used previously known values for $a_{bb_2}-a_{bb_1}=2.47\ a_0$ [37] and $a_{bf_1}=-185\ a_0$ [61] and estimated $a_{bf_2}\sim a_{bf_1}-5.1\ a_0$,where $a_0$is Bohr radius. We calculated the frequency shift for different boson densities that are similar to what we get in the experiment (Figure 3.2). In a mean field approximation the interactions between bosons can be described by a an effective spin-spin Hamiltonian:

$$H_{eff} = \frac{J}{2}\left(\sigma_z\otimes\sigma_z\right) + \frac{h}{2}\left(\sigma_z\otimes I + I\otimes\sigma_z\right)$$

where $J=\frac{\Delta E_1+\Delta E_2}{2}$ is the boson-boson coupling and $h=\frac{\Delta E_2-\Delta E_1}{2}$ and $\Delta E_i = 4\pi\frac{\hbar^2}{m_b}\left(a_{bb_i}+a_{med_i}\right)n_b + 2\pi\hbar^2\left(\frac{1}{m_f}+\frac{1}{m_b}\right)a_{bf_i}n_f$ is the energy shift of the state $|i\rangle$.

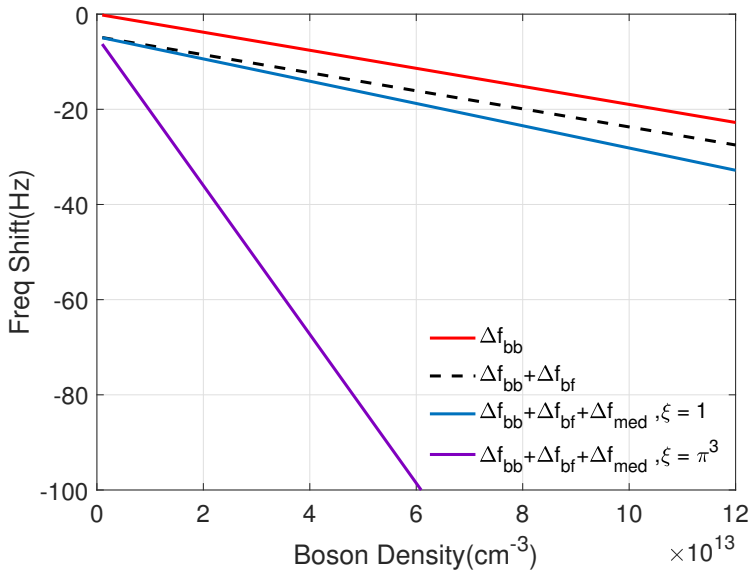

Figure 3.2: Mean-Field Frequency Shift - Frequency shift for the rubidium $|1,0\rangle \rightarrow |2,0\rangle$ transition at zero magnetic field for different boson densities, fermion density is set at $7.5 \times 10^{12} cm^{-3}$ with fermion mediated interaction (blue) and without (red). The constant shift between the lines is the boson-fermion frequency shift Δf_{bf} , the change in gradient $\frac{d\Delta f}{dn_b}$ is due to mediated interaction.

We can also calculate the frequency shift close to a boson-fermion Feshbach resonance, although mean field approximation and perturbation theory may not be valid with strong interactions. The frequency shift increases as the resonance is only relevant to one of the states. To estimate it I used the zero magnetic field scattering length for state $|2,2\rangle$ and changed the magnetic field of state $|1,1\rangle$ according to $a_{bf_1} = a_{bg}\left(1 - \frac{\Delta B}{B - B0}\right)$, a_{bg} is the zero magnetic field scattering length, B_0 the Feshbach resonance magnetic field and ΔB its width. At this moment it is not possible to get to a Feshbach resonance in our system but it is a promising future prospect, both experimentally and theoretically.

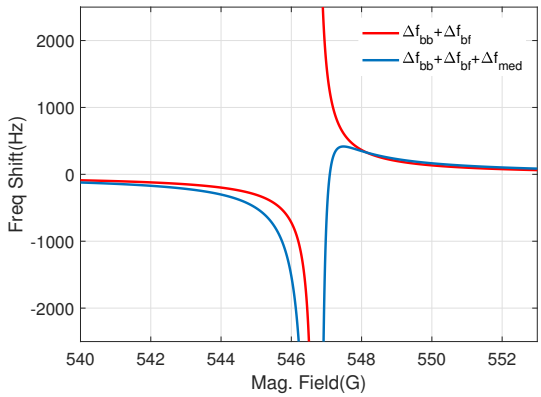

Figure 3.3: Mean-Field Frequency Shift Close to a Feshbach Resonance - Frequency shift for the rubidium $|1,1\rangle \rightarrow |2,2\rangle$ transition near a boson-fermion Feshbach resonance with fermion mediated interaction (blue) and without (red). Fermion and boson densities are constant. The shift is can reach a few kHz and more.

3.2 Experimental Results

In our experiment, a BEC of $\sim 5{\times}10^5$ ^{87}Rb atoms was in thermal contact with a DFG of $\sim 1.4{\times}10^5$ ^{40}K atoms in a crossed dipole trap of frequencies $\omega_{x,y,z} = 2\pi \times (\ 27, 39, 111)$ ($\omega_{x,y,z} = 2\pi \times (\ 29, 49, 182)$) for bosons (fermions) at a temperature of $\sim$ 90 nK ($T/T_c \sim 0.55$ and $T/T_f \sim 0.35$). The fermions are spin polarized in state$|F = 9/2, m_f = -9/2\rangle$. The mass ratio in our system is~ 2. However, since the fermions involved in the process are close to the Fermi energy ($E_f \sim K_B \cdot 260$ nK) and the BEC has a chemical potential of $\sim K_B \cdot 65$ nK, the change in fermion energy $\Delta\epsilon_f$ is larger than the change in boson energy $\Delta\epsilon_b$. For a momentum change q , smaller than the Fermi momentum k_f ,the energy change ratio is $\Delta\epsilon_f/\Delta\epsilon_b \sim \frac{m_b}{m_f}\frac{k_f}{q} \gg 1$.

We used microwave spectroscopy to measure the$|F = 1, m_f = 0\rangle = |1\rangle \leftrightarrow |F = 2, m_f = 0\rangle = |2\rangle$ hyperfine clock transition frequency in ^{87}Rb with and without^{40}K atoms. The clock transition frequency shift includes three contributions - boson-boson interaction Δf_{bb}, boson-fermion interaction Δf_{bf} and mediated interaction Δf_{med} (see eq. 3.1).

Δf_{bb} and Δf_{med} are proportional to boson density, while Δf_{bf} is independent of it. To distinguish between the three contributions, we measured frequency shifts for different boson densities, with and without fermions. With only bosons present, we measured Δf_{bb}, the change in frequency per boson density$\left(\frac{\mathrm{d}\Delta f}{\mathrm{d}n_b}\right)_b$ which is a direct measure of boson-boson interaction. When we added fermions, we measured a constant term Δf_{bf} that does not depend on boson density, and Δf_{med}, which causes change in frequency that is proportional to boson density. A change in the slope $\left(\frac{\mathrm{d}\Delta f}{\mathrm{d}n_b}\right)_{b+f}$ (measurement with bosons and fermions) compared to$\left(\frac{\mathrm{d}\Delta f}{\mathrm{d}n_b}\right)_b$ (measurement with bosons only) is a clear indication of fermion mediated interactions between bosons in our mixture.

The clock transition states are first-order magnetic insensitive at zero magnetic field and thus also

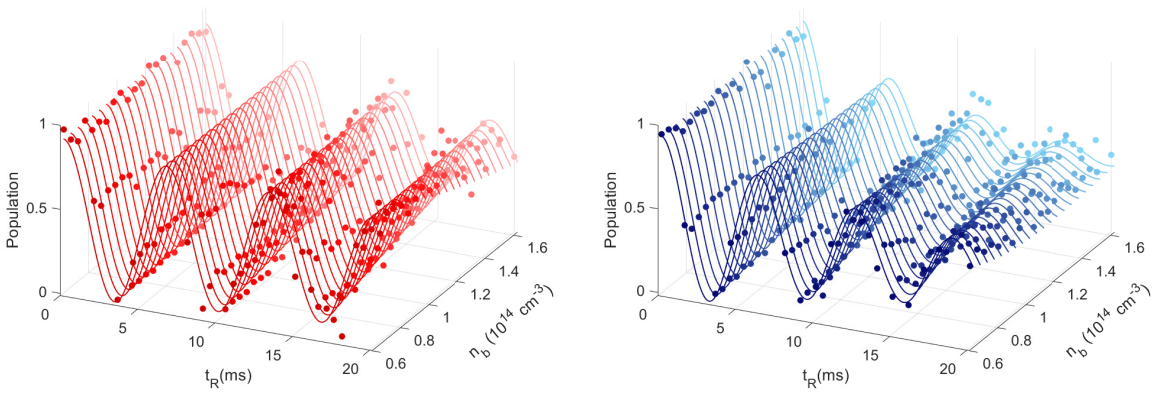

Figure 3.4: Ramsey spectroscopy - ^{87}Rb $F = 2$ population vs. Ramsey time measured at different boson densities for (a) bosons only and (b) a mixture of bosons and fermions. Data points are averaged for different boson densities to avoid cluttering (one standard deviation errors are comparable to marker size). The solid lines are the result of a single 2D fit to all data points (see eq. 3.2 in the text). We measured a boson density shift of $\left(\frac{\mathrm{d}\Delta f}{\mathrm{d}n_b}\right)_b = 12.8 \pm 2.2^{stat} \pm 2.7^{sys} \times 10^{14}\ Hz/cm^3$ for bosons (a) and $\left(\frac{\mathrm{d}\Delta f}{\mathrm{d}n_b}\right)_{b+f} = 18.5 \pm 2.5^{stat} \pm 2.2^{sys} \times 10^{14}\ Hz/cm^3$ for the boson-fermion mixture (b), this change is a clear effect of spin-spin mediated interaction. The signal decays when increasing boson density in both cases, and to a larger extent when fermions are present, another indication of mediated interactions.

have the same electronic triplet and singlet components when colliding with another atom. This renders the difference in scattering lengths $a_{bf_2} - a_{bf_1}$ between these two states small as compared with other transitions [62, 63] and thus decreases the mediated interaction shift Δf_{med} and the boson-fermion shift Δf_{bf}.

Following a Ramsey experiment of variable duration t_R, we released the atoms from the dipole trap. After a long time-of-flight (20 ms for the bosons and 12 ms for the fermions) we used absorption imaging to measure $P = N_2/N_{tot}$, the boson population in state $|2\rangle$, and the BEC chemical potential and the fermion fugacity, which we used to determine boson and fermion densities in each run. We controlled the boson density during state preparation, by transferring a pre-determined fraction of^{87}Rb atoms to state $|2\rangle$, and removing this fraction from the trap using a resonant laser pulse. Measurements without fermions were performed in an identical fashion to obtain similar boson densities, expelling the fermions at the end of preparation stage, immediately before the Ramsey measurement.

Our results are shown in Figure 3.4. Red (Blue) filled circles show the measured populations without (with) fermions. Solid lines are the result of a maximum likelihood fit to the data using the fit function:

$$P(n_b, t_R) = Ae^{-g_c n_b t_R} \cos\left((\delta + g n_b) t_R\right) + C. \tag{3.2}$$

Here, A is the contrast, g_c is decoherence rate per boson density, δ is detuning between the MW

driving field and the transition,$g = \frac{\mathrm{d}\Delta f}{\mathrm{d}n_b}$ is the boson density frequency shift, and C is a constant term to account for a finite population in state $|2\rangle$. Previous works have shown different decay parameters for Ramsey coherence [64,65], calculated for a thermal cloud of cold atoms and without collisions, while we use a BEC where the main source of decoherence are inhomogeneous density related frequency shifts. We extracted three frequency shifts from the fits. The boson density shift in the absence of fermions, Δf_{bb}, the mean-field shift due to direct boson-fermions collisions, Δf_{bf}, and the boson density shift which was mediated by the presence of fermions, Δf_{med}.

The measured frequencies and decay rates are shown in Figure 3.5. Red (Blue) lines show the result from our fit function (eq. (2)) without (with) fermions. Filled circles show frequencies taken from a fit function $P(t_R) = Ae^{-\Gamma t_R}\cos(2\pi f t_R) + C$ to averaged data for different densities. Here, A is the contrast, Γ is decay rate, f is oscillation frequency, and C is a constant term to account for a finite population in state $|2\rangle$.

Since the light shifts, local-oscillator detuning and Zeeman shifts are independent of the presence of fermions, the difference in frequency between measurements with and without fermions is a result of boson-fermion density shift $\delta_{b+f} - \delta_b = \Delta f_{bf}$. Our frequency measurements (Figure 3.5 (a)) show a constant shift with respect to boson density from which we calculate a boson-fermion scattering length difference $a_{bf_2} - a_{bf_1} = -4.66 \pm 0.26^{stat} \pm 2.20^{sys}\ a_0$ where a_0 is Bohr radius (statistical errors reported are of one standard deviation). To the best of our knowledge, the scattering length for $^{87}Rb -^{40} K$ collisions is only previously known from Feshbach spectroscopy measurement [61]. Our measured value is a correction to the low-energy elastic approximation [62,63] and can be used to calibrate inter atomic potential calculations.

When measuring without fermions, g is a direct measurement of $\frac{\Delta f_{bb}}{n_b}$. We measure a shift that corresponds with $a_{bb_2} - a_{bb_1} = -1.67 \pm 0.29^{stat} \pm 0.35^{sys}\ a_0$, in agreement with previously measured values [36,38] (after taking into account a factor of 2 for BEC statistics [66] and uncertainties in atom numbers).

When adding fermions we measure a change in the slope $\frac{\mathrm{d}\Delta f}{\mathrm{d}n_b}$ by a factor $\eta = 1.41 \pm 0.06^{stat} \pm 0.17^{sys}$ compared to a our measurement without fermions, which is a clear indication of spin-spin mediated interactions. Our measurements were done in a randomized fashion, interlacing different boson densities with/without fermions. Any systematic errors we have regarding our estimation of boson densities is common in both measurements. The slope ratio $\eta = \left(\frac{\mathrm{d}\Delta f}{\mathrm{d}n_b}\right)_{b+f} / \left(\frac{\mathrm{d}\Delta f}{\mathrm{d}n_b}\right)_b = 1 + \frac{\Delta f_{med}}{\Delta f_{bb}}$ only depends weakly on the fermion density ($\eta - 1 \propto n_f^{1/3}$). When using our measured values for $a_{bf_2} - a_{bf_1}$ and a previously known value for $a_{bf_1} = -185 \pm 7\ a_0$ [61] we calculate the expected mediated interaction shift and find $\xi = 1.28 \pm 0.13^{stat} \pm 0.35^{sys}$, in good agreement with $\xi = 1$ theory [1] and a recent mechanical measurement [4].

The measured decay rates are shown in Figure 3.5 (b). Our coherence time is limited by inhomogeneous density shifts in the BEC, previous Ramsey measurements with thermal clouds and at lower densities have shown longer coherence times ($> 0.5s$). Our results show (Figure 3.5 (b)) a clear dependence of the decay rate on the boson density. When adding the fermions the decay is faster and it also increases more rapidly with boson density by a factor of 2.5 ± 0.4. For a BEC immersed in a

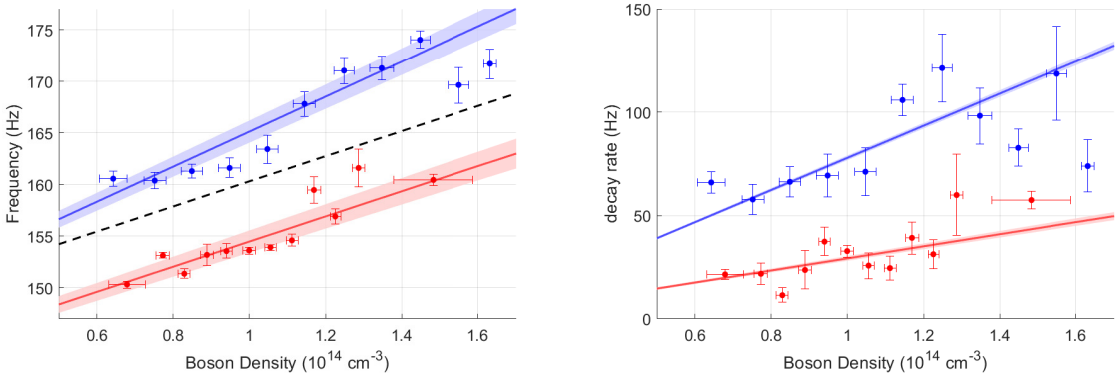

Figure 3.5: Frequency shift (a) and decay rate (b) for different boson densities for bosons only (red) and and a mixture of bosons and fermions (blue). The lines are extracted from a 2D fit to all data points (shaded area denotes one standard deviation), the filled circles are extracted from fits to averaged data for different boson densities. A dashed black line is shown in (a) parallel to red line and crosses the blue line at zero density. (a) A constant frequency shift between the two lines (i.e. independent of boson density) is a measure of boson-fermion interaction with $a_{bf_2} - a_{bf_1} = -4.66 \pm 0.26^{stat} \pm 2.20^{sys}\ a_0$. A change in the slope by a factor $\eta = 1.41 \pm 0.06^{stat} \pm 0.17^{sys}$ is a clear effect of fermion mediated interaction. Both of these effects are insensitive to any systematic error that is common to measurements with/without fermions (i.e. light shift, magnetic field fluctuations and errors in estimating the boson density). (b) The decay rate increases with boson density in both cases (with/without fermions), while the increase is faster when fermions are present. Indicating mediated interactions.

homogeneous cloud of fermions, the coherence decay should not be affected by direct collisions with the fermions. However, fermion mediated interactions should affect the decay as it changes the effective scattering length between the bosons in an in-homogeneous manner. We also note that, besides inhomogeneous density broadening, the spin-dependent coupling of bosonic superposition to a bath of fermions is expected to lead to increased decoherence, as an intrinsic aspect of mediated interactions. The change in the derivative of the decay rate with respect to boson density is another indication of mediated interactions in the mixture, as was seen in early observations of RKKY interactions in solids [9].

Chapter 4

Twisting the Bloch Sphere with Unbalanced Dynamic Decoupling

This chapter details our recent measurements of interactions in a BEC, using an unbalanced dynamic decoupling scheme with MW pulses. We measure a mean field interaction that is due to inter-states collisions. Our dynamic decoupling scheme keeps the coherence in the BEC for long times in the presence of inhomogeneous density shifts and strong magnetic noises. Unlike other similar schemes, we do not need to add another modulation to measure the interactions, as the differences in populations creates a phase shift which is automatically modulated in the dynamic decoupling sequence. We measure scattering length differences for three MW transitions, two of them are sensitive to magnetic noise. Our results can be used to observe polaron physics, to generate spin squeezing and to calibrate atomic interaction potentials.

4.1 Theoretical Background

Interactions play a primary role in ultracold gases, from the cooling process to changing the ground state of the system and driving quantum phase transitions. In the cold collision regime interaction strength is parameterized by an s-wave scattering length a_{ij}, where $|i\rangle, |j\rangle$ are two internal states of the interacting atoms (i.e. Zeeman states or hyperfine levels). Our knowledge of these interactions comes from spectroscopic measurements [36,66,67], position of Feshbach resonances [61,68] and thermalization experiments [69,70], which are then taken into account in detailed calculations of inter-atomic potentials [71]. While most of these methods are relevant for atoms in the same states, we present a dynamic decoupling method that enhances the contribution of interactions of atoms in different states ($i \neq j$).

Dynamic decoupling (DD) is a well established method to control a quantum state of a system and preserve its coherence for long times, it has been demonstrated in NMR, ultracold atoms, trapped ions and nitrogen vacancy centers in diamonds among other systems. It aims to decouple the system from its environment system by applying a set of spin rotations. By doing that it also decouples it from

most spin dependent signal one might be interested in. To generate a signal, one can modulate the system itself synchronously with the DD scheme [50,53], in a similar fashion to how a lock-in amplifier operates. However this modulation can generate noises that are in phase with the DD scheme, and require some control of the signal you are interested in.

We present a method for measuring interactions in ultracold gases in a noisy environment with a long coherence time and increased sensitivity to inter-states interactions. Our measurements are based on an unbalanced dynamic decoupling scheme that accumulates the effect of inter-states interactions between two internal states ultracold atoms without adding any modulation besides the DD itself. Precise knowledge of inter-states interaction parameters is important for interactions with impurities in the system (i.e. polarons) [11–14], spinor BECs [72] and magnons [73]. It can also be used to calibrate theoretical models of inter-atomic potentials [71, 74].

We use a Bose-Einstein condensate (BEC) of ultracold ^{87}Rb atoms in states $|1\rangle = |F = 1, m_{f_1}\rangle$ and $|2\rangle = |F = 2, m_{f_2}\rangle$, where F is the total spin of the atom and$m_{f_{1,2}}$ is the spin projection on the magnetic field axis. In the mean field approximation the two levels have energy shifts:

$$\begin{aligned} \delta E_1 &= \frac{4\pi\hbar^2}{m}(\alpha_{11}a_{11}n_1 + \alpha_{12}a_{12}n_2), \\ \delta E_2 &= \frac{4\pi\hbar^2}{m}(\alpha_{22}a_{22}n_2 + \alpha_{12}a_{12}n_1) \end{aligned} \tag{4.1}$$

here, $n_{1,2}$ are the densities in the different states, a_{ij} are the s-wave scattering lengths, m is the atoms mass, $\hbar$ is the reduced Planck constant and α_{ij} are correlation factors to account for Bose statistics. When the atoms are in a coherent superposition during the interrogation time, $\alpha_{ij} = 2$ for a thermal cloud and $\alpha_{ij} = 1$ for a BEC [66]. The energy difference between the two states in a BEC is:

$$\delta E_2 - \delta E_1 = \frac{2\pi\hbar^2}{m}((a_{22} - a_{11})(n_2 + n_1) + (a_{22} + a_{11} - 2a_{12})(n_2 - n_1)). \tag{4.2}$$

Our DD scheme takes advantage of the fact that the first term is proportional to the total density $n = n_1 + n_2$ while the second one is proportional to the density difference $\delta n = n_2 - n_1$. A typical Ramsey experiment starts with the atoms in state $|1\rangle$ and then a $\pi/2$ pulse transfers the atoms to the state $\frac{1}{\sqrt{2}}(|1\rangle + |2\rangle)$. During the interrogation time the population in the two states is equal, which makes the second term cancel out and the phase between the two state depends only on the total density. However, we can start with a non-zero density difference by applying a pulse with polar angle θ which transfers the atoms to the state $\cos\frac{\theta}{2}|1\rangle + \sin\frac{\theta}{2}|2\rangle$, here the density difference is $\delta n = n\left(\sin^2\frac{\theta}{2} - \cos^2\frac{\theta}{2}\right) = -n\cos\theta$. After time T we apply a second pulse of $\pi - \theta$ to convert the phase difference between the two states to population $P = \frac{N_2}{N_1+N_2}$,where $N_{1,2}$ is the occupation of that state. In our unbalanced DD scheme (Figure4.1 (a)) we apply a number of echo pulses N_e between the two Ramsey pulses of θ and $\pi - \theta$, with alternating phase of $0°, 90°$ to rotate the state around X, Y axis in the Bloch sphere. Rotating the Bloch vector this way cancels out noises in the control pulses and also makes the vector spend equal times in the upper and lower halves of the Bloch sphere in any block of $XYXY$ rotations. This makes any phase accumulated due to population imbalance during

the pulses nullify for finite pulse times.

This scheme cancels out the total density term and other external noises, which allows for a longer coherence time and increases sensitivity to density difference. The state of each atom evolves according to :

$$M = e^{\frac{i}{2}(\pi-\theta)(\sigma_x\cos\phi+\sigma_y\sin\phi)}\left(e^{\frac{i}{2\hbar}\sigma_z\left((g_{12}-g_{11})\cos^2\frac{\theta}{2}+(g_{22}-g_{12})\sin^2\frac{\theta}{2}\right)nT}\ e^{\frac{i}{2}\sigma_y\pi}\right.$$
$$\left.* e^{\frac{i}{2\hbar}\sigma_z\left((g_{22}-g_{12})\cos^2\frac{\theta}{2}+(g_{12}-g_{11})\sin^2\frac{\theta}{2}\right)n\cdot 2T}e^{\frac{i}{2}\sigma_x\pi}\ e^{\frac{i}{2\hbar}\sigma_z\left((g_{12}-g_{11})\cos^2\frac{\theta}{2}+(g_{22}-g_{12})\sin^2\frac{\theta}{2}\right)nT}\right)^{N_e/2}\ e^{\frac{i}{2}\sigma_x\theta} \tag{4.3}$$

here σ_i are the Pauli matrices, $g_{ij} = \frac{4\pi\hbar^2}{m}a_{ij}$, and ϕ is the phase of the last pulse (sets the axis of rotation for that operation).

The population at the end of this sequence is given by:

$$P = \frac{1}{4}\left[2\sin^2\theta\cos\left(\phi - \frac{\delta g n}{\hbar}N_e T\cos\theta\right) + \cos 2\theta + 3\right], \tag{4.4}$$

where and $\delta g = \frac{4\pi\hbar^2}{m}\left(a_{11}+a_{22}-2a_{12}\right)$ is the interaction shift. This results in a twisted Bloch sphere (Figure4.1 (b)) , where the upper hemisphere rotates in one direction and the lower hemisphere rotates in the opposite direction due to the interaction $\delta g\delta n$. This method can be used for spin squeezing, similar to [39], due to the long coherence time in our scheme we can generate a spin squeezed state even with weak interactions. It is also relevant for polaron physics, where a minority of atoms in state $|1\rangle$ interact strongly with with a majority of atoms in state $|2\rangle$. The strong interaction acts to dress the minority atoms and and they act as quasi-particles, known as polarons. The lifetime and energy of polarons have been observed recently in several mixtures, Bose mixture [12], Fermi mixture [13,14] and a Bose-Fermi mixture [11]. Our method can be used to increase coherence in these measurements, which will increase the spectroscopic resolution. It can also be useful to see how the system changes when going for a minority of atoms in one state (polarons) to equal superposition, which is achieved be scanning θ in our scheme.

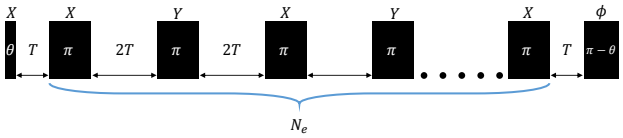

(a)

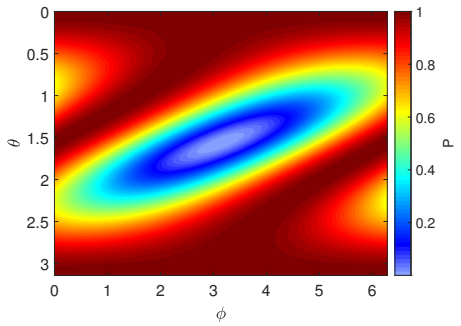

(b)

Figure 4.1: Unbalanced dynamic decoupling scheme - (a) An initial pulse of angle θ, followed by a set of N_e echo pulses around X,Y axis, separated by time $2T$, with a final pulse of angle $\pi-\theta$ and phase ϕ. The initial pulse creates a superposition $\cos\frac{\theta}{2}|1\rangle+\sin\frac{\theta}{2}|2\rangle$, with density difference $\delta n = n\left(\sin^2\frac{\theta}{2}-\cos^2\frac{\theta}{2}\right)$, where n is the total density. (b) calculated population P in state $|2\rangle$ after the sequence, while changing the phase and length of the final pulse, ϕ and θ respectively. Due to mean field interactions the phase difference between the states after the sequence is $\frac{4\pi\hbar}{m}\left(a_{11}+a_{22}-2a_{12}\right)\delta n N_e T$, where a_{11}, a_{22}, a_{12} are the s wave scattering lengths between the states.

4.2 Experimental Results

In our system we trap a BEC of $\sim 5\times10^5$ ^{87}Rb atoms in an harmonic trap with trapping frequencies of $(\omega_x,\omega_y\omega_z) = 2\pi\times(31,37,109)$ Hz. We use MW radiation with 6.834 GHz frequency to drive transition between different hyperfine levels, $|F=1,m_f=0\rangle \leftrightarrow |F=2,m_f=0\rangle$ clock transition or $|F=1,m_f=1\rangle \leftrightarrow |F=2,m_f=0\rangle$ magnetic sensitive transition, in a magnetic field of 2.067 G. We perform an unbalanced dynamic decoupling scheme as follows, we start with all atoms in the state $|1\rangle$ and apply a MW pulse to rotate the vector around the x axis with a polar angle $\theta=\Omega t_p$ in the Bloch sphere, where Ω is the Rabi frequency of our MW radiation and t_p is the pulse length. We let the state evolve for a time T and apply a MW π pulse to invert populations. After another holding time of 2T we apply a $-\pi$ pulse, and after another hold time T we apply a final pulse to rotate the vector with a polar angle $\pi-\theta$ and phase ϕ relative to the first pulse. The X,Y echo pulses can be repeated many times to accumulate more phase and increase sensitivity, we use up to 72 pulses.

At the end of the sequence we release the cloud from the trap and let it expand for 20 ms. We take two images with imaging light resonant with $F=2\rightarrow F'=3$ transition. In the first image we count only the atoms in the state $|2\rangle$ and after a short repump pulse to transfer all atoms from $F=1$ to the $F=2$ manifold, we count all the atoms in the second image. We measure the Thomas-Fermi radius

of the cloud in the second image to calculate the chemical potential and density of the BEC.

In figure 4.2 (a-d) we show the result of our measurement on the clock transition for 6 echoes with arm time $T = 3$ ms, as we change the values of θ and ϕ. The coherence is high, as no significant decay is seen in a balanced dynamical decoupling (Figure 4.2 (a)). When we change θ the contrast decreases, as expected from eq. 4.4, we see clear fringes in all cases (Figure 4.2 (b-d)) with excellent agreement with a fit to $C\cos(\phi + \Delta\phi) + B$, here C is the contrast, ϕ is the phase of our last pulse, $\Delta\phi$ is the phase shift, and B is the bias. The phase shift is visible in all measurements, and we can see it is linear with respect to δn (Figure 4.2 (e)). We can also fit all the data to a 2D fit according to eq. 4.4 and see a twisted Bloch sphere (Figure 4.2 (f)).

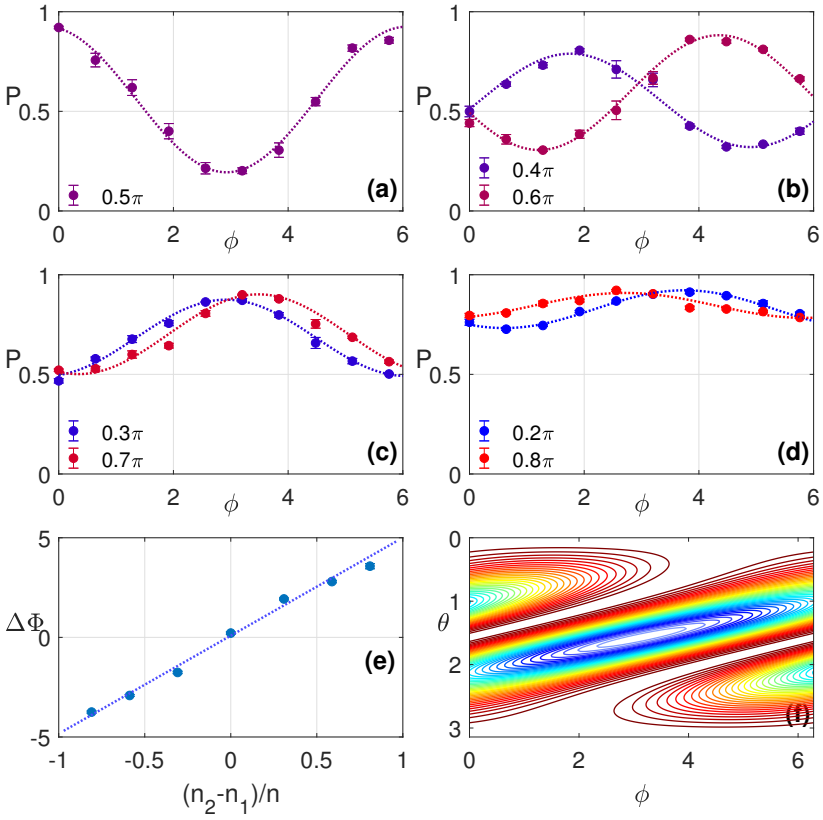

Figure 4.2: Experimental results for $|1,0\rangle \leftrightarrow |2,0\rangle$ transition after 16 echo pulses with arm time $T = 3$ ms. Measured population P while scanning the phase of the last pulse (a-d) for different θ (initial density difference $\propto \cos\theta$), showing clear fringes, dotted lines are fits to the data. The fringes are phase shifted, due to interactions and density difference δn. The phase is proportional to δn (e), as can be seen from a linear fit (dotted line). A 2D fit to all data (following eq. 4.4) shows a twisted bloch sphere (f).

We repeated this measurement for different times $T_{tot} = 2N_eT$ with different arm times T and

number of echoes N_e. The frequency shift we measure $\Delta f = \frac{\Delta\Phi}{2\pi T_{tot}}$ grows linearly with the density difference (Figure 4.3). From a linear fit we get $(a_{11} + a_{22} - 2a_{12})_{1,0\to 2,0} = 1.10 \pm 0.02\ a_0$ (statistical error of one standard deviation), an accurate measurement of this scattering length difference. Using calculated values for $a_{11} = 94.69 \pm 0.12\ a_0$ [74] and previously measured $a_{22} - a_{11} = -1.67 \pm 0.29\ a_0$ in our setup (see chapter 3) , we can get $a_{12} = 93.30 \pm 0.16\ a_0$ and $\frac{a_{11}+a_{22}-2a_{21}}{a_{22}-a_{11}} = -0.66 \pm 0.19$ which is insensitive to systematic errors in estimating density. Our measurement time is limited by inelastic collisions of atoms in state $|F = 2, m_f = 0\rangle$, transferring them to states $|F = 2, m_f = -1\rangle$ and $|F = 2, m_f = 1\rangle$.

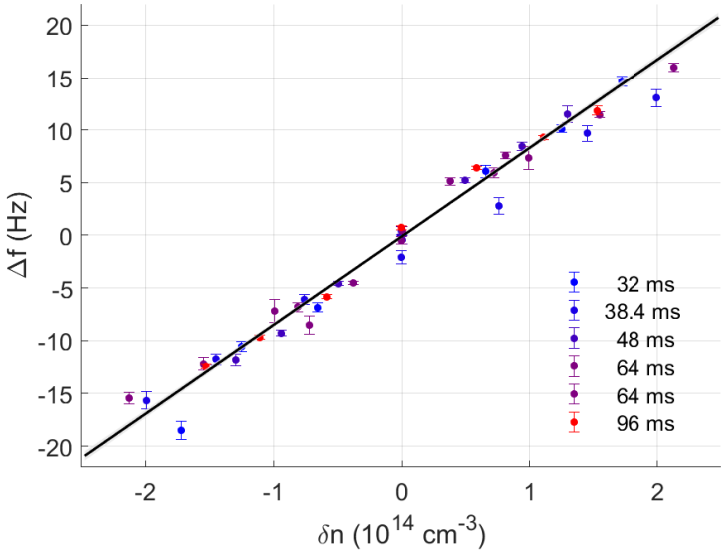

Figure 4.3: Frequency shift due to interactions - The measured frequency shift $\Delta f = \frac{\Delta\Phi}{2\pi T_{tot}}$ from many measurements of unbalanced dynamic decoupling with different number of echo pulses and arm times. Color scale indicates the total time of each measurement. A linear fit to the data (black line, with one standard deviation in gray) gives a scattering length difference of $(a_{11} + a_{22} - 2a_{12})_{1,0\to 2,0} = 1.10 \pm 0.02\ a_0$, showing the high accuracy that can be acheived in this method.

Our dynamic decoupling scheme can be used to cancel external noises that are slower than our pulse rate $1/T$. To test it we perform the same measurement on two magnetic sensitive transitions, $|F = 1, m_f = 1\rangle \leftrightarrow |F = 2, m_f = 0\rangle$ and $|F = 1, m_f = 1\rangle \leftrightarrow |F = 2, m_f = 2\rangle$ with a magnetic field sensitivity of 0.7 kHz/mG and 2.1 kHz/mG respectively. Using Ramsey spectroscopy synchronized to the 50 Hz signal of the electricity grid in our lab we measured the magnetic noise at 50 Hz to be of 0.89 mG peak to peak. To cancel this noise we use dynamic decoupling with shorter arm time T of $0.35 - 0.42$ ms with the magnetic sensitive transitions. Our results for these transitions (Figure4.4) show long coherence times and a phase shift that is proportional to the density difference δn.

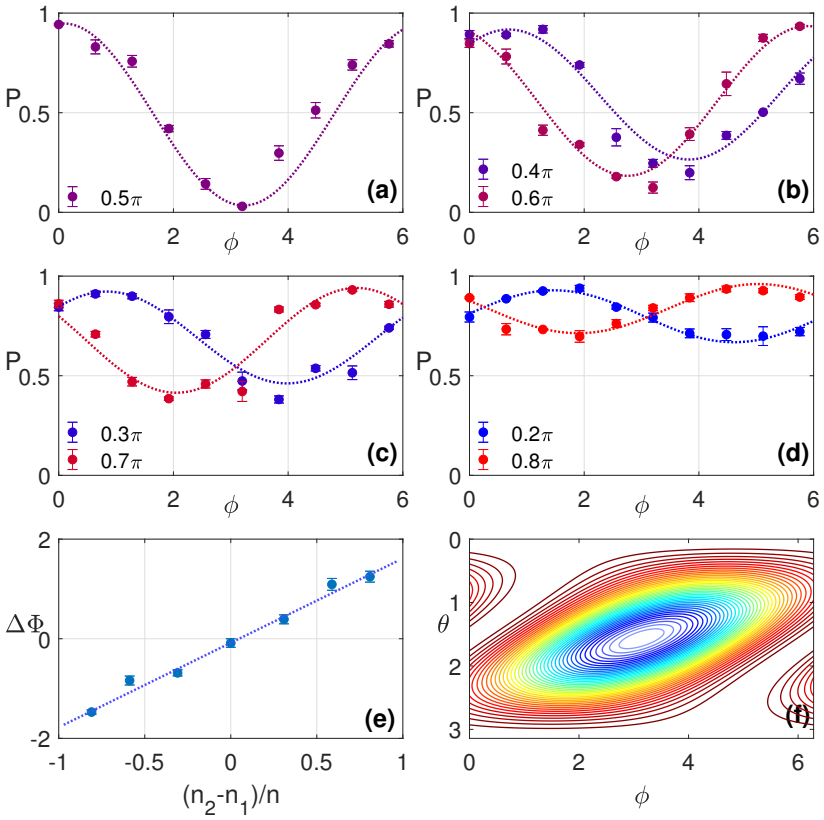

Figure 4.4: Experimental results for $|1,1\rangle \leftrightarrow |2,0\rangle$ transition after 56 echo pulses with arm time $T = 0.42$ ms. Measured population P while scanning the phase of the last pulse (a-d) for different θ (initial density difference $\propto \cos\theta$), showing clear fringes. The short arm time T is needed to keep a high coherence in the presence of strong magnetic noises. The fringes are phase shifted, due to interactions and density difference δn. The phase is proportional to δn (e), as can be seen from a linear fit (dotted line). A 2D fit to all data (following eq. 4.4) shows a twisted bloch sphere (f).

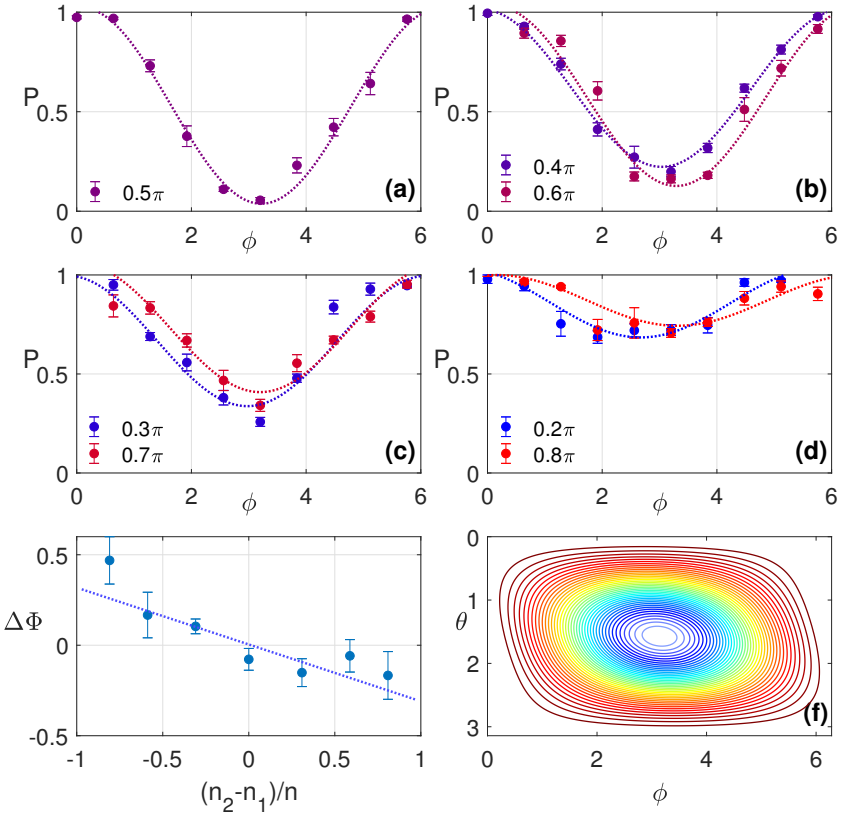

Figure 4.5: Experimental results for $|1,1\rangle \leftrightarrow |2,2\rangle$ transition after 48 echo pulses with arm time $T = 0.35$ ms. Measured population P while scanning the phase of the last pulse (a-d) for different population imbalance $-\cos\theta$, showing clear fringes. The short arm time T is needed to keep a high coherence in the presence of strong magnetic noises, we use many pulses to accumulate enough phase shift. The fringes are phase shifted, due to interactions and density difference δn. The phase is proportional to δn (e), as can be seen from a linear fit (dotted line). A 2D fit to all data (following eq. 4.4) shows a twisted Bloch sphere (f).

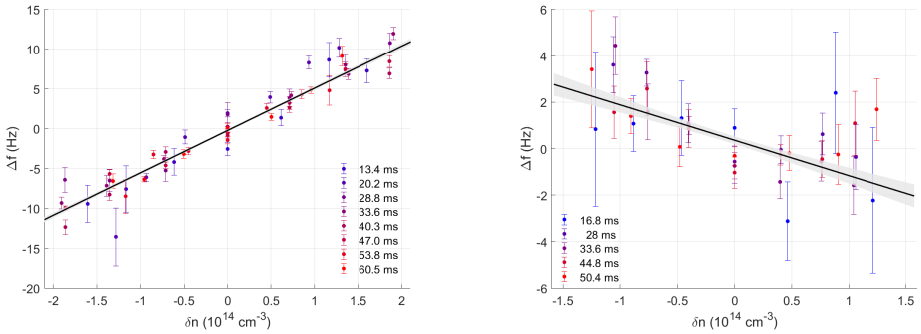

Figure 4.6: Frequency shift due to interactions in magnetic transitions - The measured frequency shift Δf from many measurements of unbalanced dynamic decoupling with different number of echo pulses and arm times for $|1,1\rangle \leftrightarrow |2,0\rangle$(a) and $|1,1\rangle \leftrightarrow |2,2\rangle$ (b) . Color scale indicates the total time of each measurement. A linear fit to the data (black line, with one standard deviation in gray) gives a scattering length difference of (a) $(a_{11}+a_{22}-2a_{12})_{1,1\to 2,0} = 0.69 \pm 0.02\ a_0$ and (b)$(a_{11}+a_{22}-2a_{12})_{1,1\to 2,2} = -0.20 \pm 0.04\ a_0$ showing the high signal to noise that can be acheived in this method even in the presence of strong magnetic noise.

Similarly to our experiments on the the clock transition, we repeated these measurements for different times T_{tot} with different arm times T and number of echoes N_e, and measured a frequency shift Δf that grows linearly with the density difference (Figure 4.6). From a linear fit we get $(a_{11}+a_{22}-2a_{21})_{1,1\to 2,0} = 0.69 \pm 0.02\ a_0$ for the $|1,1\rangle \leftrightarrow |2,0\rangle$ transition, and $(a_{11}+a_{22}-2a_{21})_{1,1\to 2,2} = -0.20 \pm 0.04\ a_0$ for the $|1,1\rangle \leftrightarrow |2,2\rangle$ transition, showing good signal to noise even in a noisy environment.

Our measurements demonstrate a novel method for measuring interactions in ultracold atoms, which can be relevant for other systems where dynamic decoupling is a common method , such as NV centers in diamonds or NMR experiments. Our accuracy is comparable to other measurement on another clock transition $|1,-1\rangle \leftrightarrow |2,1\rangle$ [66, 67], and extend it to magnetic sensitive transitions. The imbalanced populations interactions generate a phase shift that is accumulated in the sequence without having to externally perturb system, as done in other dynamic decoupling schemes [52, 53]. This type of interactions are of great interest in polaron physics, and can be used to increase signal to noise in ultracold atoms experiments studying this phenomena.

Chapter 5

Summary and Outlook

We have measured mean field interactions with high precision in two different cases with different methods. Our measurement of spin-spin fermion mediated interaction is a first observation of this kind of interaction in ultracold atomic gases. It is a long range interaction that can be tuned with Feshbach resonance, these features are rather unique and can lead to new and interesting physics. Our observations are consistent with a predicted mean field effect of this interaction, and to another recent measurement of a in cold atoms [4] that observed a mechanical effect caused by fermion mediated interactions. Our observation of a change in decay rate when adding the fermions is an indication of the effect of mediated interactions on coherence in our mixture. To make it more quantitative we need a better theory, that takes into account inhomogeneous shifts in our mixture, perhaps solving a coupled Gross-Pitaevski equation, similar to [67].

To observe a stronger effect we can use another transition where the change in boson-fermion interaction are larger which will lead to a larger effect of mediated interaction. Such transitions are usually magnetic sensitive since their electron triplet and singlet spin components are different (in clock transitions they are equal), which requires significantly decreasing the magnetic noise in our lab, or working with dynamic decoupling scheme to measure this effect.

We have recently begun experimenting with an interleaved dynamic decoupling scheme (figure 5.1 (a)), where we use echo pulses to flip the populations of the bosons and increase coherence, and synchronously flip the spin of the fermions surrounding them. In this manner, the boson-fermion interaction before the echo pulse is different from after the echo pulse and a phase shift is created due to this change - $\Delta\phi = \underbrace{\hbar\left(\frac{1}{m_f}+\frac{1}{m_b}\right)\left(\left(a^{bf}_{2,\downarrow}-a^{bf}_{2,\uparrow}\right)-\left(a^{bf}_{1,\downarrow}-a^{bf}_{1,\uparrow}\right)\right)n_f T}_{\Delta\phi_{bf}} + \underbrace{2\frac{\hbar}{m_b}\left(\left(a^{med}_{2,\downarrow}-a^{med}_{2,\uparrow}\right)-\left(a^{med}_{1,\downarrow}-a^{med}_{1,\uparrow}\right)\right)n_b T}_{\Delta\phi_{med}}$.
From our calculations, the frequency shift in this scheme should be of a few 10s of Hz. Our preliminary results (figure 5.1 (b)) have shown a shift but are not stable and consistent yet.

To measure an effect beyond mean field, we should increase the interactions by going close to a Feshbach resonance, where a perturbative theory is not applicable and a more advanced theory is needed, which makes it a more interesting problem for experimentalist to work on. While theoretical

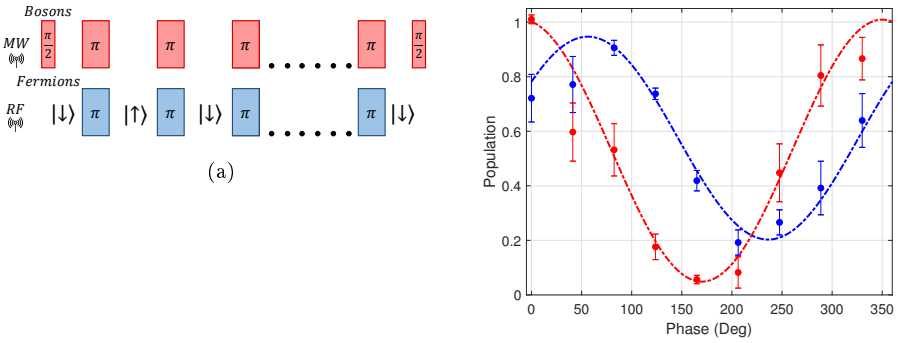

(a) (b)

Figure 5.1: Interleaved Dynamic Decoupling - (a) The pulse scheme used, MW pulses flips the populations of the bosons between states $|1,1\rangle$ and $|2,2\rangle$. RF pulses change the population of the fermions from $|\downarrow\rangle = |9/2,-9/2\rangle \leftrightarrow |\uparrow\rangle = |9/2,+9/2\rangle$, where the scattering length a_{bf} is different. (b) Experimental results for 12 echo pulses with total time 9.6 ms and a phase shift of $\Delta\phi = -40.08 \pm 6.7$ between the red curve (no RF pulses) and the blue curve (with RF pulses) which amounts to a frequency shift of -34.8 Hz . The dynamic decoupling preserves a full coherence even though there is a strong 50 Hz noise, as described in chapter 2.

suggestions [2, 3] focused on using this interaction to reach new phases of matter in a lattice or a bi-layer configuration, even in a simple configuration in a harmonic trap , we don't have a clear idea of how it will look like.

Our measurement of interactions in a BEC using unbalanced dynamic decoupling shows a novel method to isolate a specific term in the interactions between two states of a BEC, without adding another external modulation besides the dynamic decoupling pulses. We have used it to measure this interaction term with high accuracy and long coherence time with a weak interaction. We have measured interaction shift of a few Hz between magnetic sensitive states, overcoming a magnetic noise of a few kHz, demonstrating the ability to overcome external noises and isolate a specific interaction term with this method.

It can also be useful when the interactions are strong. Using this method in that regime, experiments of spin squeezing, such as [39], can achieve longer coherence times with a stronger on-axis twist of the Bloch sphere, and higher spin squeezing. Polaron physics also becomes relevant close to a Feshbach resonance [11–14], as it deals with the energy and lifetime of a minority of atoms in a strongly interacting environment. Other systems where dynamic decoupling is intensively used, such as NV centers and NMR, can also be interesting to look at with this method.

There is a possibility to combine these two measurements and measure mediated interactions with unbalanced dynamic decoupling. This is an interesting prospect, as the dynamic decoupling cancels any boson-fermion interaction, so any change in interactions when adding the fermions can be attributed to mediated interactions. We have tried to measure it in our lab already with no indication of mediated interaction yet, however , we do not have any prediction on the scale of this shifts and if they are detectable in our system.

Our current efforts are towards getting our mixture close to the Feshbach resonance, where beyond mean field physics can be observed and dynamic decoupling can be a useful tool since it cancels out external noises, and magnetic noises should be dominant in that region.

Bibliography

[1] DH Santamore and Eddy Timmermans. Fermion-mediated interactions in a dilute bose-einstein condensate. *Physical Review A*, 78(1):013619, 2008.

[2] S De and IB Spielman. Fermion-mediated long-range interactions between bosons stored in an optical lattice. *Applied Physics B*, 114(4):527–536, 2014.

[3] Daniel Suchet, Zhigang Wu, Frédéric Chevy, and Georg M Bruun. Long-range mediated interactions in a mixed-dimensional system. *Physical Review A*, 95(4):043643, 2017.

[4] BJ DeSalvo, Krutik Patel, Geyue Cai, and Cheng Chin. Observation of fermion-mediated interactions between bosonic atoms. *Nature*, 568(7750):61, 2019.

[5] Hagai Edri, Boaz Raz, Noam Matzliah, Nir Davidson, and Roee Ozeri. Observation of spin-spin fermion-mediated interactions between ultra-cold bosons. *arXiv preprint arXiv:1910.01341*, 2019.

[6] Melvin A Ruderman and Charles Kittel. Indirect exchange coupling of nuclear magnetic moments by conduction electrons. *Physical Review*, 96(1):99, 1954.

[7] Tadao Kasuya. A theory of metallic ferro-and antiferromagnetism on zener's model. *Progress of theoretical physics*, 16(1):45–57, 1956.

[8] Kei Yosida. Magnetic properties of cu-mn alloys. *Physical Review*, 106(5):893, 1957.

[9] N Bloembergen and TJ Rowland. On the nuclear magnetic resonance in metals and alloys. *Acta metallurgica*, 1(6):731–746, 1953.

[10] J Friedel. Xiv. the distribution of electrons round impurities in monovalent metals. *The London, Edinburgh, and Dublin Philosophical Magazine and Journal of Science*, 43(337):153–189, 1952.

[11] Ming-Guang Hu, Michael J Van de Graaff, Dhruv Kedar, John P Corson, Eric A Cornell, and Deborah S Jin. Bose polarons in the strongly interacting regime. *Physical review letters*, 117(5):055301, 2016.

[12] Nils B Jørgensen, Lars Wacker, Kristoffer T Skalmstang, Meera M Parish, Jesper Levinsen, Rasmus S Christensen, Georg M Bruun, and Jan J Arlt. Observation of attractive and repulsive polarons in a bose-einstein condensate. *Physical review letters*, 117(5):055302, 2016.

[13] Christoph Kohstall, Mattheo Zaccanti, Matthias Jag, Andreas Trenkwalder, Pietro Massignan, Georg M Bruun, Florian Schreck, and Rudolf Grimm. Metastability and coherence of repulsive polarons in a strongly interacting fermi mixture. *Nature*, 485(7400):615, 2012.

[14] André Schirotzek, Cheng-Hsun Wu, Ariel Sommer, and Martin W. Zwierlein. Observation of fermi polarons in a tunable fermi liquid of ultracold atoms. *Phys. Rev. Lett.*, 102:230402, Jun 2009.

[15] M. H. Anderson, J. R. Ensher, M. R. Matthews, C. E. Wieman, and E. A. Cornell. Observation of bose-einstein condensation in a dilute atomic vapor. *Science*, 269(5221):198–201, 1995.

[16] K. B. Davis, M. O. Mewes, M. R. Andrews, N. J. van Druten, D. S. Durfee, D. M. Kurn, and W. Ketterle. Bose-einstein condensation in a gas of sodium atoms. *Phys. Rev. Lett.*, 75(22):3969–3973, Nov 1995.

[17] Martin W Zwierlein, Christian H Schunck, André Schirotzek, and Wolfgang Ketterle. Direct observation of the superfluid phase transition in ultracold fermi gases. *nature*, 442(7098):54, 2006.

[18] Igor Ferrier-Barbut, Marion Delehaye, Sebastien Laurent, Andrew T Grier, Matthieu Pierce, Benno S Rem, Frédéric Chevy, and Christophe Salomon. A mixture of bose and fermi superfluids. *Science*, 345(6200):1035–1038, 2014.

[19] Markus Greiner, Olaf Mandel, Tilman Esslinger, Theodor W Hänsch, and Immanuel Bloch. Quantum phase transition from a superfluid to a mott insulator in a gas of ultracold atoms. *nature*, 415(6867):39, 2002.

[20] Mingyang Guo, Fabian Böttcher, Jens Hertkorn, Jan-Niklas Schmidt, Matthias Wenzel, Hans Peter Büchler, Tim Langen, and Tilman Pfau. The low-energy goldstone mode in a trapped dipolar supersolid. *arXiv preprint arXiv:1906.04633*, 2019.

[21] G. Natale, R. M. W. van Bijnen, A. Patscheider, D. Petter, M. J. Mark, L. Chomaz, and F. Ferlaino. Excitation spectrum of a trapped dipolar supersolid and its experimental evidence. *Phys. Rev. Lett.*, 123:050402, Aug 2019.

[22] L Tanzi, SM Roccuzzo, E Lucioni, F Famà, A Fioretti, C Gabbanini, G Modugno, A Recati, and S Stringari. Supersolid symmetry breaking from compressional oscillations in a dipolar quantum gas. *arXiv preprint arXiv:1906.02791*, 2019.

[23] Anton Mazurenko, Christie S Chiu, Geoffrey Ji, Maxwell F Parsons, Márton Kanász-Nagy, Richard Schmidt, Fabian Grusdt, Eugene Demler, Daniel Greif, and Markus Greiner. A cold-atom fermi–hubbard antiferromagnet. *Nature*, 545(7655):462, 2017.

[24] Jae-yoon Choi, Sebastian Hild, Johannes Zeiher, Peter Schauß, Antonio Rubio-Abadal, Tarik Yefsah, Vedika Khemani, David A Huse, Immanuel Bloch, and Christian Gross. Exploring the many-body localization transition in two dimensions. *Science*, 352(6293):1547–1552, 2016.

[25] Alexander Lukin, Matthew Rispoli, Robert Schittko, M Eric Tai, Adam M Kaufman, Soonwon Choi, Vedika Khemani, Julian Léonard, and Markus Greiner. Probing entanglement in a many-body–localized system. *Science*, 364(6437):256–260, 2019.

[26] Michael Schreiber, Sean S Hodgman, Pranjal Bordia, Henrik P Lüschen, Mark H Fischer, Ronen Vosk, Ehud Altman, Ulrich Schneider, and Immanuel Bloch. Observation of many-body localization of interacting fermions in a quasirandom optical lattice. *Science*, 349(6250):842–845, 2015.

[27] Ph Courteille, RS Freeland, DJ Heinzen, FA Van Abeelen, and BJ Verhaar. Observation of a feshbach resonance in cold atom scattering. *Physical review letters*, 81(1):69, 1998.

[28] S Inouye, MR Andrews, J Stenger, H-J Miesner, DM Stamper-Kurn, and W Ketterle. Observation of feshbach resonances in a bose–einstein condensate. *Nature*, 392(6672):151–154, 1998.

[29] Leticia Tarruell, Daniel Greif, Thomas Uehlinger, Gregor Jotzu, and Tilman Esslinger. Creating, moving and merging dirac points with a fermi gas in a tunable honeycomb lattice. *Nature*, 483(7389):302, 2012.

[30] Gregor Jotzu, Michael Messer, Rémi Desbuquois, Martin Lebrat, Thomas Uehlinger, Daniel Greif, and Tilman Esslinger. Experimental realization of the topological haldane model with ultracold fermions. *Nature*, 515(7526):237, 2014.

[31] Peter T Brown, Debayan Mitra, Elmer Guardado-Sanchez, Reza Nourafkan, Alexis Reymbaut, Charles-David Hébert, Simon Bergeron, A-MS Tremblay, Jure Kokalj, David A Huse, et al. Bad metallic transport in a cold atom fermi-hubbard system. *Science*, 363(6425):379–382, 2019.

[32] Waseem S Bakr, Jonathon I Gillen, Amy Peng, Simon Fölling, and Markus Greiner. A quantum gas microscope for detecting single atoms in a hubbard-regime optical lattice. *Nature*, 462(7269):74, 2009.

[33] Lawrence W Cheuk, Matthew A Nichols, Melih Okan, Thomas Gersdorf, Vinay V Ramasesh, Waseem S Bakr, Thomas Lompe, and Martin W Zwierlein. Quantum-gas microscope for fermionic atoms. *Physical review letters*, 114(19):193001, 2015.

[34] Elmar Haller, James Hudson, Andrew Kelly, Dylan A Cotta, Bruno Peaudecerf, Graham D Bruce, and Stefan Kuhr. Single-atom imaging of fermions in a quantum-gas microscope. *Nature Physics*, 11(9):738, 2015.

[35] Richard P Feynman. Simulating physics with computers. *International journal of theoretical physics*, 21(6):467–488, 1982.

[36] Chad Fertig and Kurt Gibble. Measurement and cancellation of the cold collision frequency shift in an 87 rb fountain clock. *Physical review letters*, 85(8):1622, 2000.

[37] Kurt Gibble and Steven Chu. Laser-cooled cs frequency standard and a measurement of the frequency shift due to ultracold collisions. *Physical review letters*, 70(12):1771, 1993.

[38] Y. Sortais, S. Bize, C. Nicolas, A. Clairon, C. Salomon, and C. Williams. Cold collision frequency shifts in a ^{87}Rb atomic fountain. *Phys. Rev. Lett.*, 85:3117–3120, Oct 2000.

[39] Christian Gross, Tilman Zibold, Eike Nicklas, Jerome Esteve, and Markus K Oberthaler. Nonlinear atom interferometer surpasses classical precision limit. *Nature*, 464(7292):1165, 2010.

[40] Yusuke Nishida. Phases of a bilayer fermi gas. *Physical Review A*, 82(1):011605, 2010.

[41] Herbert Fröhlich, Hans Pelzer, and Sigurd Zienau. Xx. properties of slow electrons in polar materials. *The London, Edinburgh, and Dublin Philosophical Magazine and Journal of Science*, 41(314):221–242, 1950.

[42] Asif Sinay. *PhD Thesis*. PhD thesis, Weizmann Institute of Science, 2016.

[43] Noam Matzliah. *PhD Thesis*. PhD thesis, Weizmann Institute of Science, 2018.

[44] S Aubin, S Myrskog, MHT Extavour, LJ LeBlanc, D McKay, A Stummer, and JH Thywissen. Rapid sympathetic cooling to fermi degeneracy on a chip. *Nature Physics*, 2(6):384–387, 2006.

[45] Dt Haar. *Fluctuation, Relaxation and Resonance in Magnetic Systems: Scottish Universities' Summer School 1961*. Oliver & Boyd, 1962.

[46] Ulrich Haeberlen. *High Resolution NMR in Solids: Advances in Magnetic Resonance*. Academic Press, 1976.

[47] Ryogo Kubo and Kazuhisa Tomita. A general theory of magnetic resonance absorption. *Journal of the Physical Society of Japan*, 9(6):888–919, 1954.

[48] Jiangfeng Du, Xing Rong, Nan Zhao, Ya Wang, Jiahui Yang, and RB Liu. Preserving electron spin coherence in solids by optimal dynamical decoupling. *Nature*, 461(7268):1265, 2009.

[49] G De Lange, ZH Wang, D Riste, VV Dobrovitski, and R Hanson. Universal dynamical decoupling of a single solid-state spin from a spin bath. *Science*, 330(6000):60–63, 2010.

[50] Shlomi Kotler, Nitzan Akerman, Yinnon Glickman, Anna Keselman, and Roee Ozeri. Single-ion quantum lock-in amplifier. *Nature*, 473(7345):61, 2011.

[51] Shlomi Kotler, Nitzan Akerman, Yinnon Glickman, and Roee Ozeri. Nonlinear single-spin spectrum analyzer. *Physical review letters*, 110(11):110503, 2013.

[52] Ravid Shaniv, Nitzan Akerman, and Roee Ozeri. Atomic quadrupole moment measurement using dynamic decoupling. *Physical review letters*, 116(14):140801, 2016.

[53] Ravid Shaniv and Roee Ozeri. Quantum lock-in force sensing using optical clock doppler velocimetry. *Nature communications*, 8:14157, 2017.

[54] Michael J Biercuk, Hermann Uys, Aaron P VanDevender, Nobuyasu Shiga, Wayne M Itano, and John J Bollinger. Optimized dynamical decoupling in a model quantum memory. *Nature*, 458(7241):996, 2009.

[55] Yoav Sagi, Ido Almog, and Nir Davidson. Process tomography of dynamical decoupling in a dense cold atomic ensemble. *Physical review letters*, 105(5):053201, 2010.

[56] Ido Almog, Yoav Sagi, Goren Gordon, Guy Bensky, Gershon Kurizki, and Nir Davidson. Direct measurement of the system–environment coupling as a tool for understanding decoherence and dynamical decoupling. *Journal of Physics B: Atomic, Molecular and Optical Physics*, 44(15):154006, 2011.

[57] E. L. Hahn. Spin echoes. *Phys. Rev.*, 80:580–594, Nov 1950.

[58] Götz S. Uhrig. Keeping a quantum bit alive by optimized π-pulse sequences. *Phys. Rev. Lett.*, 98:100504, Mar 2007.

[59] Ashok Ajoy, Gonzalo A. Álvarez, and Dieter Suter. Optimal pulse spacing for dynamical decoupling in the presence of a purely dephasing spin bath. *Phys. Rev. A*, 83:032303, Mar 2011.

[60] ST Chui and VN Ryzhov. Collapse transition in mixtures of bosons and fermions. *Physical Review A*, 69(4):043607, 2004.

[61] Francesca Ferlaino, Chiara DErrico, Giacomo Roati, Matteo Zaccanti, Massimo Inguscio, Giovanni Modugno, and Andrea Simoni. Feshbach spectroscopy of a k- rb atomic mixture. *Physical Review A*, 73(4):040702, 2006.

[62] R Côté, A Dalgarno, H Wang, and WC Stwalley. Potassium scattering lengths and prospects for bose-einstein condensation and sympathetic cooling. *Physical Review A*, 57(6):R4118, 1998.

[63] Alexander Dalgarno and MRH Rudge. Spin-change cross-sections for collisions between alkali atoms. *Proceedings of the Royal Society of London. Series A. Mathematical and Physical Sciences*, 286(1407):519–524, 1965.

[64] S. Kuhr, W. Alt, D. Schrader, I. Dotsenko, Y. Miroshnychenko, A. Rauschenbeutel, and D. Meschede. Analysis of dephasing mechanisms in a standing-wave dipole trap. *Phys. Rev. A*, 72:023406, Aug 2005.

[65] Yehonatan Dallal and Roee Ozeri. Measurement of the spin-dipolar part of the tensor polarizability of ^{87}Rb. *Phys. Rev. Lett.*, 115:183001, Oct 2015.

[66] DM Harber, HJ Lewandowski, JM McGuirk, and Eric A Cornell. Effect of cold collisions on spin coherence and resonance shifts in a magnetically trapped ultracold gas. *Physical Review A*, 66(5):053616, 2002.

[67] M Egorov, B Opanchuk, P Drummond, BV Hall, P Hannaford, and AI Sidorov. Measurement of s-wave scattering lengths in a two-component bose-einstein condensate. *Physical Review A*, 87(5):053614, 2013.

[68] Aaron Bennett, Kurt Gibble, Servaas Kokkelmans, and Jeremy M. Hutson. Atomic clock measurements of quantum scattering phase shifts spanning feshbach resonances at ultralow fields. *Phys. Rev. Lett.*, 119:113401, Sep 2017.

[69] C. Marzok, B. Deh, Ph. W. Courteille, and C. Zimmermann. Ultracold thermalization of ^{7}Li and ^{87}Rb. *Phys. Rev. A*, 76:052704, Nov 2007.

[70] G. Ferrari, M. Inguscio, W. Jastrzebski, G. Modugno, G. Roati, and A. Simoni. Collisional properties of ultracold k-rb mixtures. *Phys. Rev. Lett.*, 89:053202, Jul 2002.

[71] B. J. Verhaar, E. G. M. van Kempen, and S. J. J. M. F. Kokkelmans. Predicting scattering properties of ultracold atoms: Adiabatic accumulated phase method and mass scaling. *Phys. Rev. A*, 79:032711, Mar 2009.

[72] Dan M. Stamper-Kurn and Masahito Ueda. Spinor bose gases: Symmetries, magnetism, and quantum dynamics. *Rev. Mod. Phys.*, 85:1191–1244, Jul 2013.

[73] G. Edward Marti, Andrew MacRae, Ryan Olf, Sean Lourette, Fang Fang, and Dan M. Stamper-Kurn. Coherent magnon optics in a ferromagnetic spinor bose-einstein condensate. *Phys. Rev. Lett.*, 113:155302, Oct 2014.

[74] EGM Van Kempen, SJJMF Kokkelmans, DJ Heinzen, and BJ Verhaar. Interisotope determination of ultracold rubidium interactions from three high-precision experiments. *Physical review letters*, 88(9):093201, 2002.

[75] Noam Matzliah, Hagai Edri, Asif Sinay, Roee Ozeri, and Nir Davidson. Observation of optomechanical strain in a cold atomic cloud. *Physical review letters*, 119(16):163201, 2017.

Appendix A - Published Papers

During my PhD i worked on three main topics, two of them are described in the thesis, and an article on the third one [75] is presented below.

List of publications:

1. Noam Matzliah*, Hagai Edri*, Asif Sinay, Roee Ozeri, and Nir Davidson. Observation of optomechanical strain in a cold atomic cloud. Physical review letters, 119(16):163201, 2017.

2. Hagai Edri, Boaz Raz, Noam Matzliah, Nir Davidson, and Roee Ozeri. Observation of spin-spin fermion-mediated interactions between ultra-cold bosons. arXiv preprint arXiv:1910.01341, 2019. (detailed in chapter 3)

3. Hagai Edri, Boaz Raz, Roee Ozeri, and Nir Davidson, Twisting the Bloch Sphere with Unbalanced Dynamic Decoupling - *in preparation*. (detailed in chapter 4).

* Equal contributors.

Observation of Optomechanical Strain in a Cold Atomic Cloud

Noam Matzliah, Hagai Edri, Asif Sinay, Roee Ozeri, and Nir Davidson
Department of Physics of Complex Systems, Weizmann Institute of Science, Rehovot 7610001, Israel
(Received 15 June 2017; revised manuscript received 10 August 2017; published 19 October 2017; corrected 23 October 2017)

We report the observation of optomechanical strain applied to thermal and quantum degenerate ^{87}Rb atomic clouds when illuminated by an intense, far detuned homogeneous laser beam. In this regime the atomic cloud acts as a lens that focuses the laser beam. As a backaction, the atoms experience a force opposite to the beam deflection, which depends on the atomic cloud density profile. We experimentally demonstrate the basic features of this force, distinguishing it from the well-established scattering and dipole forces. The observed strain saturates, ultimately limiting the momentum impulse that can be transferred to the atoms. This optomechanical force may effectively induce interparticle interactions, which can be optically tuned.

DOI: 10.1103/PhysRevLett.119.163201

Light-matter interactions are at the core of cold atom physics. A laser beam illuminating atoms close to atomic resonance frequency will apply a scattering force on them, and an inhomogeneous laser beam far from resonance will mainly apply an optical dipole force [1]. An intense, far detuned homogeneous laser beam does not exert a significant force on a single atom, though when applied on inhomogeneous atomic clouds, it will. This was pointed out [2] while studying lensing by cold atomic clouds in the context of nondestructive imaging.

The atom's electric polarizability makes atomic clouds behave as refractive media with an index locally dependent on the cloud density. An atomic cloud thus behaves as a lens that can focus or defocus the laser beam. The atoms recoil in the opposite direction to the beam deflection due to momentum conservation. In solid lenses, this optomechanical force causes a small amount of stress with negligible strain, due to their rigidity. An atomic lens, however, deforms, making the force on the atoms observable by imaging their strain. We refer to this optomechanical force as electrostriction, since it resembles shape changes of materials under the application of a static electric field. Electrostriction can be viewed as an optically induced force between atoms, since the force each atom experiences depends on the local density of the other atoms.

Optomechanical forces are applied in experiments on refractive matter mainly by optical tweezers, pioneered by [3], using structured light. Less commonly, such forces can be applied by homogeneous light using angular momentum conversion due to the material birefringence [4], or using structured refractive material shapes [5]. Optomechanical forces implemented by such techniques are used for optically translating and rotating small objects. By applying electrostriction on cold atoms we gain access to the effect of optical strain—an aspect in optomechanics not directly studied yet in spite of its importance in current research [6].

Interactions between cold atoms can appear naturally or be externally induced and tuned. Tuning is mostly done using a magnetic Feshbach resonance, which was used to demonstrate many important physical effects such as Bose-Einstein condensate (BEC) collapse and explosion [7], Feshbach molecules [8,9], BEC-BCS crossover in strongly interacting degenerate fermions [10–12], and Fermi superfluidity [13–16]. Interactions are also tuned by optical Feshbach resonance [17], optical cavities [18], or radio frequency Feshbach resonance [19]. Interactions can be induced by shining a laser beam on the atoms and creating a feedback mechanism to their response by an externally pumped cavity or a half cavity [20–25]. The electrostriction force reported here is a new kind of induced force between atoms, and may be useful in cold atoms and quantum degenerate atom experiments.

In this Letter we analyze and measure for the first time the optomechanical strain induced in a cold atomic cloud by a homogeneous laser beam far detuned from atomic resonance. We shine the beam on the cloud and directly observe the resulting strain after time of flight by absorption imaging. We show that this is a new kind of light-induced force acting on cold atoms. A saturation of the strain is observed, which depends only on the ratio between the momentum impulse applied to the atomic cloud and the initial momentum distribution width of the cloud. Possible implications for this new force are suggested, and, in particular, light-induced interaction tuning.

With respect to laser light far from resonance, an inhomogeneous atomic cloud behaves as a lens [2], as predicted by the optical Bloch equations. When a plane wave passes through the cloud, it acquires a position-dependent phase $\phi(\vec{r})$. If the phase is small, the Poynting vector direction changes [26] by an angle $|\vec{\nabla}_\perp \phi|/k_L$, where $\vec{\nabla}_\perp$ is the gradient along the two directions perpendicular to the laser beam propagation direction, and k_L, the wave number of the beam. As a backaction, the atomic

momentum changes in the opposite direction. The momentum change of the atoms is associated with the electrostriction force, which takes the form [27]

$$\vec{f}_{\rm es} = \frac{\hbar\Gamma^2}{8\Delta}\frac{I}{I_s}\frac{\vec{\nabla}_\perp n}{n} = -\vec{\nabla}_\perp U_{\rm es}$$
$$U_{\rm es} = -\frac{\hbar\Gamma^2}{8\Delta}\frac{I}{I_s}\ln\left(\frac{n}{n_0}\right), \quad (1)$$

where n_0 is an arbitrarily chosen constant density that fixes the arbitrariness in defining a potential up to a constant, Γ, the width of the atomic transition, Δ, the detuning of the laser, I, its intensity, I_s, the ^{87}Rb saturation intensity, and n, the local density of atoms.

This force acts only in the directions transverse to the beam propagation and is derived from a potential in the transverse directions that scale logarithmically with the density. It is a collective force in the sense that it acts only on atoms consisting of an inhomogeneous atomic cloud. The laser induces interactions between the atoms and the resulting force is independent of the number of atoms. The force scales as I/Δ, similar to the dipole force, and unlike other light-induced interactions predicted before [31–33], which are second order in atom-light coupling. For convex clouds it is repulsive for red detuned laser $\Delta < 0$, and attractive for blue detuned laser $\Delta > 0$, opposite to the dipole force. Similar to the dipole force, changing the polarization has a small effect of coupling different atomic states, which effectively changes I_s.

In the experiment we typically trap 10^6 ^{87}Rb atoms in the $|F = 1, m_F = 1\rangle$ ground state of the $5^2S_{1/2}$ manifold at a temperature of $T = 400$ nK. Our crossed dipole trap has typical trap frequencies of $\omega_x = \omega_y = 2\pi \times 45$ Hz and $\omega_z = 2\pi \times 190$ Hz. The atomic cloud, when illuminated by a red detuned laser beam with $\Delta = -100$ GHz, is optically equivalent to a graded index lens of Gaussian profile $e^{-x^2/(2\sigma_z^2)-y^2/(2\sigma_y^2)-z^2/(2\sigma_z^2)}$. Its peak refractive index is $n_{\rm ref} = 1.0000093$ and its widths are $\sigma_x = \sigma_y = 22$ μm, and $\sigma_z = 5.2$ μm. To generate the electrostriction force we use a $\lambda = 780$ nm laser, 50–200 GHz detuned from the $|F = 2\rangle \to |F' = 3\rangle$ transition. The beam is coupled to a polarization maintaining single mode fiber and ejects with a waist of 1.1 mm. Under these parameters, the dipole force associated with the laser beam itself is suppressed by 10^{-3} compared to the electrostriction force, and the scattering probability is only a few percent. The dipole force that the light focused by the atoms exerts on the atoms is negligible. The electrostriction beam is shone from the $\hat{y}$ direction (see Fig. 1). The atomic cloud is optically extended ($\sigma \gg \lambda$), so a simple refractive media treatment is adequate. It is dilute ($nk^{-3} = 0.25$), so dipole-dipole interatomic interactions [34,35] do not affect our experiment. To measure the force we apply a short pulse of duration τ_p right after releasing the cloud, and image the momentum distribution after a long expansion time [18 ms, Figs. 1(a)–1(c)] by absorption imaging along the $\hat{z}$ direction. Since the force is

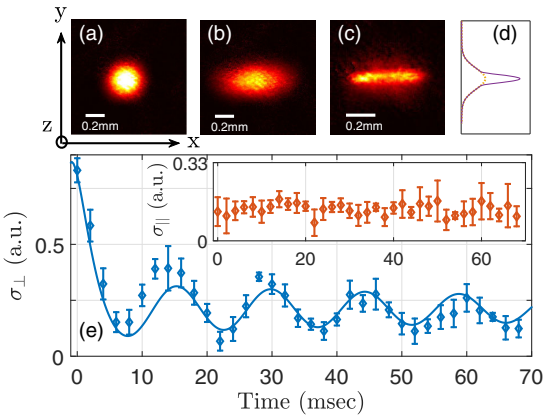

FIG. 1. Strain measurements. Absorption image of a thermal cloud after long expansion times with (b) and without (a) an electrostriction pulse. The cloud aspect ratio changes from unity to 2.1. We used a laser beam shone along the $\hat{y}$ axis with intensity 8×10^3 mW/cm^2, detuning 47 GHz and pulsed for 0.5 ms. (c) A BEC after an electrostriction pulse and long expansion time. Even for a strong impulse and large aspect ratio the BEC remains partly condensed, showing a bimodal distribution in the axial direction (d). (e) Oscillations in the cloud size along one transverse direction (axial direction shown in inset) induced by an electrostriction pulse as a function of a variable waiting time in the trap after applying the pulse. A pure transverse breathing mode is observed, fitting to a decaying oscillation (solid line) of twice the trap frequency.

anisotropic, the cloud expands more in the transverse directions and gains an aspect ratio (AR) larger than unity. If the atoms do not move during the pulse (impulse approximation, $\tau_p \ll \omega^{-1}$) we can calculate the atomic cloud size σ along the transverse ($\perp$) and axial ($\parallel$) directions after time of flight. For a cloud with initial temperature T and after expansion time t,

$$\sigma_\perp = \sqrt{\frac{k_B T}{m\omega_\perp^2}}\sqrt{\left(1 - \frac{\hbar\Gamma}{k_B T}\frac{\Gamma}{8\Delta}\frac{I}{I_s}\omega_\perp^2 t\tau_p\right)^2 + \omega_\perp^2 t^2},$$
$$\sigma_\parallel = \sqrt{\frac{k_B T}{m\omega_\parallel^2}}\sqrt{1 + \omega_\parallel^2 t^2}. \quad (2)$$

After a long expansion time the aspect ratio $\sigma_\perp/\sigma_\parallel$ of the cloud reaches an asymptotic value,

$${\rm AR}^2 = 1 + \left(\frac{\hbar\Gamma}{k_B T}\frac{\Gamma}{8\Delta}\frac{I}{I_s}\omega_\perp\tau_p\right)^2 = 1 + \left(\frac{\sigma_P^{\rm es}}{\sigma_P^{\rm th}}\right)^2, \quad (3)$$

where $\sigma_P^{\rm es} = (\hbar\Gamma\sqrt{m}/\sqrt{k_B T})(\Gamma/8\Delta)(I/I_s)\omega_\perp\tau_p$ is the momentum distribution width of the electrostriction impulse, and $\sigma_P^{\rm th} = \sqrt{mk_B T}$, the width of the initial cloud thermal momentum distribution.

The above derivation relies on the impulse approximation. In order to check its validity, we numerically solved the dynamics of the atomic cloud when applying electrostriction on it using a phase-space simulation. The simulation results coincide with our analytic predictions for all

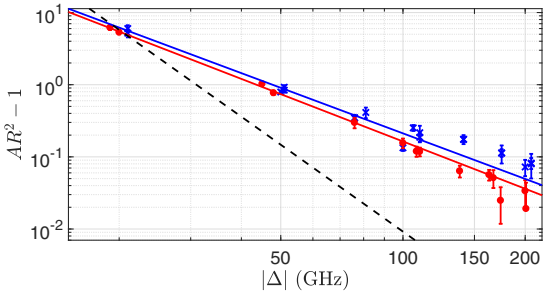

FIG. 2. Scaling of strain with detuning Δ. A thermal cloud AR after an electrostriction pulse and free expansion, red circles (blue crosses), correspond to a red (blue) detuned electrostriction laser. Fits to the data (solid lines) indicate a scaling of the force as $1/\Delta^{\alpha}$, with $\alpha = 1.09(5)$ [$\alpha = 1.05(9)$] for the red (blue) detuned electrostriction laser. A prediction (dashed line) based on a force that scales as $1/\Delta^2$ is shown as well. The error in α corresponds to a 95% confidence level. We used a cloud with a temperature of 1.1μK and a laser with intensity 1.1×10^4 mW/cm^2, pulsed for 0.5 ms.

measurements presented here, confirming the impulse approximation. Further theoretical considerations regarding the above derivation are detailed in [27].

Performing this experiment we observe that the electrostriction pulse neither changes the cloud size along the longitudinal direction nor the center of mass [Figs. 1(a) and 1(b)]. This indicates that our experiment suffers no significant scattering and demonstrates the transverse nature of the optomechanical strain. This is more dramatically demonstrated performing the same measurement on a BEC. In this case [Fig. 1(c)] the usually fragile bimodal distribution typical of a BEC along the axial direction is unaffected by the strong momentum impulse in the transverse directions. Similar results for pure condensates prove that the force acting on the atoms is different from that predicted in [33]. We nevertheless emphasize that our predictions in Eqs. (2) and (3) do not hold for a BEC, for which the equation has to be modified.

Applying an electrostriction pulse *in situ* generates a breathing mode oscillation, only in the transverse directions. This can be observed by letting the cloud evolve in the trap for some variable time, and imaging it after release [Fig. 1(e)]. The results in Fig. 1 did not depend on the laser polarization, in accordance with our theory. This observation also indicates that the interactions we induce between atoms are not dipole-dipole interactions.

We perform strain measurements after short electrostriction pulses for a large range of detunings $|\Delta| < 200$ GHz. The results (Fig. 2) are consistent with a $1/\Delta$ rather than a $1/\Delta^2$ scaling. This agrees with our prediction in Eq. (1) and rules out the scattering force and the forces in [32,33], which scale as $1/\Delta^2$, as a source of the strain observed. Imaging the cloud a short time after the electrostriction impulse we observe the effect of the detuning's sign as well [27].

To qualitatively compare our observations to the theoretical prediction [Eq. (2)], we carefully calibrate our experimental parameters. In particular, we measured the spontaneous Raman transition rate between the $|F = 1\rangle$ and $|F = 2\rangle$ hyperfine states due to the electrostriction laser. The measured rate was in accordance with the rate calculated [27] using the Kramers-Heizenberg equation [28,36], given the independently directly measured laser intensity and detuning values, and the atomic parameters [37]. After calibration, the observed effect is roughly 2.5 times weaker than expected. As we currently do not have an explanation for this discrepancy, we scale our predictions by this factor when comparing results to theory throughout this paper (Figs. 2–4).

We further investigated the dependence of the electrostriction force on the cloud parameters: total number of atoms N and cloud size. We measured the aspect ratio, N, and the cloud size, while applying the same strain pulse on the cloud (Fig. 3 and inset). As seen, the measured AR is independent of N, as expected from Eq. (1). On the other hand, the effect shows a strong dependence on the atomic cloud size. Decreasing the cloud size makes the cloud a stronger lens, causing the beam to focus stronger and impart more momentum on the atoms.

The dipole force might, in principle, cause dependence on the cloud size if the laser beam deviates from a plane wave, suffering intensity profile changes on length scales comparable with the cloud size. In order to avoid such situations, we work with a beam size about 100 times greater than our cloud size. We avoid speckles using a single mode fiber with a collimator and no other optical elements before the vacuum cell. We verified the absence of spatial sharp intensity changes by direct imaging of the beam. The strain we observed did not change after a slight misalignment of the beam, suggesting that indeed no significant local gradients appear. This shows that the

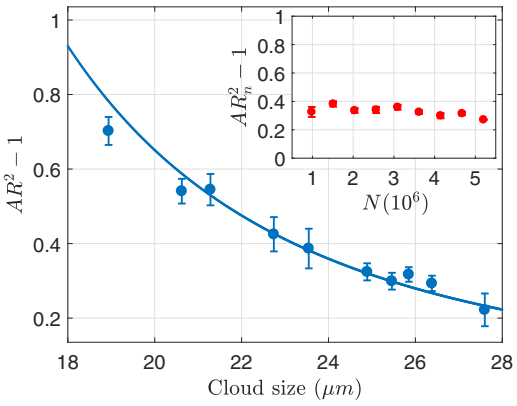

FIG. 3. Strain for clouds of different sizes. Measured cloud aspect ratio after an electrostriction pulse and free expansion for different cloud sizes (circles), and the theoretical prediction (line, scaled strain). All data points correspond to thermal clouds besides the first one, which includes a small condensed fraction. Smaller clouds consist of fewer atoms, but the AR_n (normalized AR [27]) is independent of the number of atoms as can be seen in the inset. We used a laser with intensity 7.4×10^3 mW/cm^2 and detuning 73 GHz, pulsed for 0.25 ms.

observed cloud size dependence is not due to a dipole force of the electrostriction beam.

In order to verify the linearity of the electrostriction force strength with intensity I, we measured the strain as a function of growing optical power and different pulse durations and detunings. As seen in Figs. 4(a) and 4(b), linearity is indeed evident for low intensities. However, a clear saturation of the strain [Figs. 4(a)–4(c)] occurs at high intensities, for various electrostriction pulse durations and detunings. We measured the dependence of saturation on the cloud temperature as well (not shown in Fig. 4), and found it appears to depend on the impulse applied to the atomic cloud $I\tau_p/(T\Delta)$. This is evident from the collapse of all data on a single curve as in Fig. 4. We note that the results presented in Figs. 2 and 3 were performed for unsaturated strain.

The saturation of the effect stems neither from changes in the internal state of the atoms nor from expansion of the cloud during the pulse. Our pulses are considerably short (up to 1 ms) compared with the trap oscillation period of typically 20 ms and the scattering rate of 20 Hz. We verified that there are no changes in the cloud density and internal state by imaging the cloud at short times and measuring the number of atoms in the $|F = 1\rangle$ hyperfine state. The only evident change is the momentum distribution of the atoms, which should not affect the strain via our theory. As is clear from Fig. 4(c), saturation occurs when the atoms have accelerated to a momentum roughly equal to their initial thermal velocity spread, $\sigma_P^{\mathrm{es}} = \sigma_P^{\mathrm{th}}$.

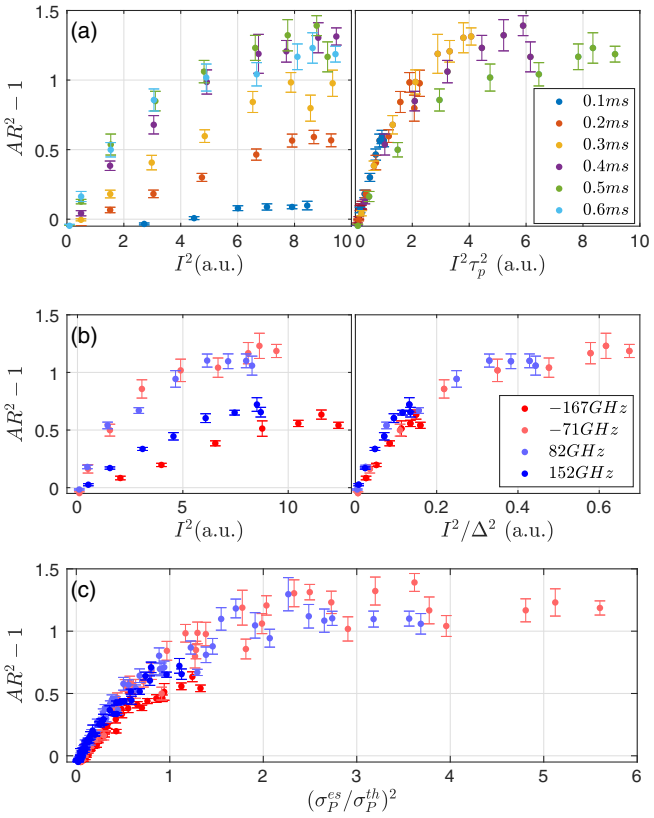

FIG. 4. Strain saturation with electrostriction laser intensity I, detuning Δ and pulse duration τ_p. (a) Saturation with laser intensity I for different pulse durations τ_p (left graph). After scaling the results by τ_p^2 (right) they collapse to a single curve. (b) Saturation with laser intensity I for different detunings Δ (left graph). After scaling the results by Δ^2 (right) they collapse to a single curve. (c) When plotted as a function of the momentum impulse σ_P^{es}, all measurements collapse together. The laser intensity is changed between $0 - 9 \times 10^3$ mW/cm^2, the detuning Δ between $(-167) - (+152)$ GHz, and the pulse duration τ_p between 0.1 and 0.6 ms. σ_P^{th} is the width of the thermal momentum distribution prior to the electrostriction impulse.

The observation that lensing saturates close to $\sigma_P^{\mathrm{es}} = \sigma_P^{\mathrm{th}}$ is reminiscent of a classical version of Einstein's recoiling-slit gedankenexperiment [38,39]. In this experiment an interference pattern of light that passed scatterers (slits) is dephased when the momentum imparted to the scatterers by the photons separates the scatterers in momentum space giving away the which-path information. In our experiment, lensing occurs due to coherent interference of light passing through different parts of the cloud. In an analogy to the above gedankenexperiment, the cloud would therefore cease to behave as a coherent lens after accumulating a momentum impulse σ_P^{es} comparable to their initial momentum distribution σ_P^{th}.

The bound on the electrostriction momentum given to the atomic cloud may prevent application of electrostriction for long times. For short times, the optomechanical strain has some interesting features of potentially practical importance (details in [27]). An electrostriction laser beam applied to a BEC can effectively modify the interparticle interaction strength at the mean-field level, mimicking the effect of a Feshbach resonance, without really changing the scattering length. Interaction tuning was used before [40] for short times using an optical Feshbach resonance. A BEC with attractive effective interactions induced by an electrostriction laser is unstable to spatial density modulations seeded by initial noise in the density profile of the cloud, as in nonlinear optical fibers [41]. An atomic cloud with repulsive effective interactions works to smoothen out spatial density modulations. This can serve as an explanation to the unexplained red-blue asymmetry in [24]. The electrostriction potential [Eq. (1)] serves as a logarithmic nonlinearity, and thus a BEC under illumination can support stable solitons in any dimension [42], a nontrivial feature [43,44]. Finally, a thermal atomic cloud can be self-trapped by its own strain, resembling a bright soliton [45] in the transverse directions, incoherent and with arbitrary shape and size.

In summary, we report the observation of optomechanical strain applied to ^{87}Rb thermal and condensed atoms when illuminated by an intense, far detuned homogeneous laser beam. We experimentally demonstrate the basic features of electrostriction, distinguishing it from the well-established scattering and dipole forces, and proving that it is a new type of force acting on cold atoms. By the observed electrostriction characteristics, we point out that this force is distinct from theoretically predicted light-induced forces such as those discussed in [31–33] or collective forces measured in

[46,47]. The experimental results are in qualitative agreement with our theory. Electrostriction has the potential to be an important tool in cold atom experiments as it effectively induces interparticle interactions, which can be optically tuned.

The authors thank Igor Mazets, Gad Afek and Arnaud Courvoisier for discussions. This work was supported by the Crown Photonics Center, ICore Israeli Excellence Center Circle of Light, and the European Research Council (Consolidator Grant No. 616919).

N. M. and H. E. contributed equally to this work.

[1] C. J. Foot, *Atomic Physics* (Oxford University Press, Oxford, 2005), Vol. 7.
[2] M. R. Andrews, M.-O. Mewes, N. J. van Druten, D. S. Durfee, D. M. Kurn, and W. Ketterle, Science **273**, 84 (1996).
[3] A. Ashkin, Phys. Rev. Lett. **24**, 156 (1970).
[4] M. Friese, T. Nieminen, N. Heckenberg, and H. Rubinsztein-Dunlop, Nature (London) **394**, 348 (1998).
[5] G. A. Swartzlander Jr., T. J. Peterson, A. B. Artusio-Glimpse, and A. D. Raisanen, Nat. Photonics **5**, 48 (2011).
[6] Z. Huang, K. Cui, Y. Li, X. Feng, F. Liu, W. Zhang, and Y. Huang, Sci. Rep. **5**, 15964 (2015).
[7] E. A. Donley, N. R. Claussen, S. L. Cornish, J. L. Roberts, E. A. Cornell, and C. E. Wieman, Nature (London) **412**, 295 (2001).
[8] E. A. Donley, N. R. Claussen, S. T. Thompson, and C. E. Wieman, Nature (London) **417**, 529 (2002).
[9] C. A. Regal, C. Ticknor, J. L. Bohn, and D. S. Jin, Nature (London) **424**, 47 (2003).
[10] M. Greiner, C. A. Regal, and D. S. Jin, Nature (London) **426**, 537 (2003).
[11] C. A. Regal and D. S. Jin, Phys. Rev. Lett. **90**, 230404 (2003).
[12] C. A. Regal, M. Greiner, and D. S. Jin, Phys. Rev. Lett. **92**, 040403 (2004).
[13] D. E. Miller, J. K. Chin, C. A. Stan, Y. Liu, W. Setiawan, C. Sanner, and W. Ketterle, Phys. Rev. Lett. **99**, 070402 (2007).
[14] J. Siegl, W. Weimer, K. Morgener, K. Hueck, N. Luick, and H. Moritz, in *APS Division of Atomic, Molecular, and Optical Physics Meeting Abstracts* (2014), Vol. 1, p. 1016.
[15] I. Ferrier-Barbut, M. Delehaye, S. Laurent, A. T. Grier, M. Pierce, B. S. Rem, F. Chevy, and C. Salomon, Science **345**, 1035 (2014).
[16] M. Delehaye, S. Laurent, I. Ferrier-Barbut, S. Jin, F. Chevy, and C. Salomon, Phys. Rev. Lett. **115**, 265303 (2015).
[17] D. M. Bauer, M. Lettner, C. Vo, G. Rempe, and S. Dürr, Nat. Phys. **5**, 339 (2009).
[18] H. Ritsch, P. Domokos, F. Brennecke, and T. Esslinger, Rev. Mod. Phys. **85**, 553 (2013).
[19] Y. Ding, J. P. D'Incao, and C. H. Greene, Phys. Rev. A **95**, 022709 (2017).
[20] D. Nagy, J. Asboth, P. Domokos, and H. Ritsch, Europhys. Lett. **74**, 254 (2006).
[21] E. Tesio, G. R. M. Robb, T. Ackemann, W. J. Firth, and G.-L. Oppo, Phys. Rev. A **86**, 031801 (2012).
[22] E. Tesio, G. R. M. Robb, T. Ackemann, W. J. Firth, and G.-L. Oppo, Phys. Rev. Lett. **112**, 043901 (2014).
[23] G. R. M. Robb, E. Tesio, G.-L. Oppo, W. J. Firth, T. Ackemann, and R. Bonifacio, Phys. Rev. Lett. **114**, 173903 (2015).
[24] G. Labeyrie, E. Tesio, P. M. Gomes, G.-L. Oppo, W. J. Firth, G. R. Robb, A. S. Arnold, R. Kaiser, and T. Ackemann, Nat. Photonics **8**, 321 (2014).
[25] A. Camara, R. Kaiser, G. Labeyrie, W. J. Firth, G.-L. Oppo, G. R. M. Robb, A. S. Arnold, and T. Ackemann, Phys. Rev. A **92**, 013820 (2015).
[26] M. Born and E. Wolf, *Principles of Optics: Electromagnetic Theory of Propagation, Interference, and Diffraction of Light* (Elsevier, New York, 1980).
[27] See Supplemental Material at http://link.aps.org/supplemental/10.1103/PhysRevLett.119.163201, including Refs. [24,25,28–30], for detailed derivations, additional technical details, experimental results, and further research topics.
[28] R. Loudon, *The Quantum Theory of Light* (Oxford University Press, Oxford, 2000).
[29] P. Meystre and M. Sargent, *Elements of Quantum Optics* (Springer Science & Business Media, New York, 2013).
[30] H. Ritsch, P. Domokos, F. Brennecke, and T. Esslinger, Rev. Mod. Phys. **85**, 553 (2013).
[31] I. Mazets, Eur. Phys. J. D **8**, 371 (2000).
[32] G. Kurizki, S. Giovanazzi, D. ODell, and A. I. Artemiev, in *Dynamics and Thermodynamics of Systems with Long-Range Interactions* (Springer, New York, 2002), pp. 369–403.
[33] A. Kim, D. Cattani, D. Anderson, and M. Lisak, Sov. Phys. JETP **81** (2005).
[34] S. Balik, A. L. Win, M. D. Havey, I. M. Sokolov, and D. V. Kupriyanov, Phys. Rev. A **87**, 053817 (2013).
[35] L. Corman, J.-L. Ville, R. Saint-Jalm, M. Aidelsburger, T. Bienaimé, S. Nascimbène, J. Dalibard, and J. Beugnon, arXiv:1706.09698.
[36] R. Cline, J. Miller, M. Matthews, and D. Heinzen, Opt. Lett. **19**, 207 (1994).
[37] D. A. Steck, http://steck.us/alkalidata.
[38] P. A. Schilpp and H. Jehle, Am. J. Phys. **19**, 252 (1951).
[39] M. Jammer *The Philosophy of Quantum Mechanics: The Interpretations of Quantum Mechanics in Historical Perspective* (Wiley, New York, 1974).
[40] M. Cetina, M. Jag, R. S. Lous, I. Fritsche, J. T. Walraven, R. Grimm, J. Levinsen, M. M. Parish, R. Schmidt, M. Knap *et al.*, Science **354**, 96 (2016).
[41] K. Tai, A. Hasegawa, and A. Tomita, Phys. Rev. Lett. **56**, 135 (1986).
[42] I. Bialynicki-Birula and J. Mycielski, Bull. Acad. Polon. Sci. Cl **3**, 461 (1975).
[43] P. Pedri and L. Santos, Phys. Rev. Lett. **95**, 200404 (2005).
[44] J. W. Fleischer, M. Segev, N. K. Efremidis, and D. N. Christodoulides, Nature (London) **422**, 147 (2003).
[45] L. Khaykovich, F. Schreck, G. Ferrari, T. Bourdel, J. Cubizolles, L. Carr, Y. Castin, and C. Salomon, Science **296**, 1290 (2002).
[46] Z. Meir, O. Schwartz, E. Shahmoon, D. Oron, and R. Ozeri, Phys. Rev. Lett. **113**, 193002 (2014).
[47] J. Pellegrino, R. Bourgain, S. Jennewein, Y. R. P. Sortais, A. Browaeys, S. D. Jenkins, and J. Ruostekoski, Phys. Rev. Lett. **113**, 133602 (2014).

Declaration

I hereby declare that except where specific reference is made to the work of others, the contents of this dissertation are original and have not been submitted in whole or in part for consideration for any other degree or qualification in this, or any other university. The experiments described in this thesis were initiated and performed by myself, with the assistance of Boaz Raz and Noam Matzliah. The experiment described in appendix A, were initiated and led by Noam Matzliah and myself with the help of Asif Sinai.

Hagai Edri, December 2019